Journal of Zhejiang University SCIENCE
ISSN 1009-3095
http://www.zju.edu.cn/jzus
E-mail: jzus@zju.edu.cn

JZUS

Review:

Perspectives on the metallic interconnects for solid oxide fuel cells

ZHU Wei-zhong[1,2], YAN Mi[1]

([1]*State Key Lab of Silicon Materials, Zhejiang University, Hangzhou 310027, China*)

([2]*Research & Development Division, Nanoolynamics Inc. Buffolo, NY, 14203, USA*)

E-mail: zhuwzus@yahoo.com; mse_yanmi@dial.zju.edu.cn

Received Sept. 1, 2004; revision accepted Sept. 20, 2004

Abstract: The various stages and progress in the development of interconnect materials for solid oxide fuel cells (SOFCs) over the last two decades are reviewed. The criteria for the application of materials as interconnects are highlighted. Interconnects based on lanthanum chromite ceramics demonstrate many inherent drawbacks and therefore are only useful for SOFCs operating around 1000 °C. The advance in the research of anode-supported flat SOFCs facilitates the replacement of ceramic interconnects with metallic ones due to their significantly lowered working temperature. Besides, interconnects made of metals or alloys offer many advantages as compared to their ceramic counterpart. The oxidation response and thermal expansion behaviors of various prospective metallic interconnects are examined and evaluated. The minimization of contact resistance to achieve desired and reliable stack performance during their projected lifetime still remains a highly challenging issue with metallic interconnects. Inexpensive coating materials and techniques may play a key role in promoting the commercialization of SOFC stack whose interconnects are constructed of some current commercially available alloys. Alternatively, development of new metallic materials that are capable of forming stable oxide scales with sluggish growth rate and sufficient electrical conductivity is called for.

Key words: Solid oxide fuel cells (SOFCs), Interconnects, Metallic materials
doi:10.1631/jzus.2004.1471 **Document code:** A **CLC number:** TQ175.71^{+}1

INTRODUCTION

Last two decades have witnessed significant progress in the research and development of solid oxide fuel cells (SOFCs), driving them closer to the ultimate goal of commercialization (Kabs *et al*., 1997; Foger *et al*., 1999; deHaart *et al*., 2001; Yasuda *et al*., 2001a; Mukerjee *et al*., 2001). SOFC is a solid electrochemical device to convert chemical reaction energy directly into electrical energy without combustion process. It offers a clean, pollution-free technology to generate electricity at efficiencies considerably higher than any other types of fuel cells. In addition to being highly efficient, SOFCs have advantages over conventional energy-generating systems in terms of reliability, fuel flexibility, modularity, low emission of NO_x and SO_x pollutants, as well as environmental friendliness. They also show relatively high tolerance to trace levels of impurities in the gas stream. Since they are comprised of entirely solid components, there is no issue of materials management encountered in molten carbonate fuel cells. Furthermore, due to their high operating temperatures typically in the range of 800 °C~1000 °C, hydrocarbon fuels such as methane and natural gas can be reformed within the stack, eliminating the need for an expensive external reformer system (Hirschenhofer *et al*., 1998; Singhal, 2000). More advantageously, the high-quality byproduct heat generated in pressurized SOFCs can replace combustors in gas turbines, allowing the realization of cogener-

ated hybrid power systems. System efficiencies approaching 70% in such hybrid SOFC/gas-turbine have been demonstrated (Lunghi and Ubertini, 2001).

The operating principle of SOFCs is schematically illustrated in Fig.1. SOFCs are literally made up of two porous electrodes separated by a gas impermeable ion-conducting electrolyte. In operation, oxygen transported in the form of either air or pure oxygen electrochemically reacts with incoming electrons from the external circuit to form an oxygen ion at the cathode (air electrode). The oxygen ion migrates through the electrolyte to the electrode/anode interface where the fuel gas simultaneously fed at the anode (fuel electrode) is electrochemically oxidized to release electrons. The external electron current from anode to cathode is balanced by the internal oxygen ion current across the electrolyte. The overall area as well as electrochemical activity of three phase boundaries (TPBs), where gas, electrolyte, and electrode converge at both sides of the electrolyte, are crucial in determining the performance of SOFCs.

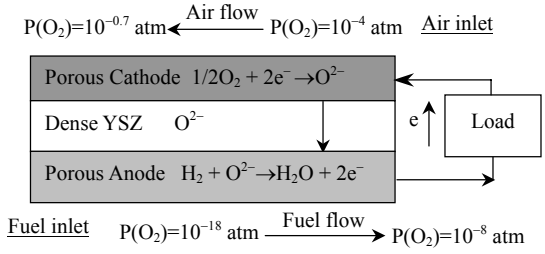

Alternative anode reactions:

$CO + O^{2-} \rightarrow CO_2 + 2e^-$

$CH_4 + 4O^{2-} \rightarrow 2H_2O + CO_2 + 8e^-$

Fig.1 Schematic drawing showing the working principle of a solid oxide fuel cell operating on hydrogen

The actual cell voltage is always lower than the theoretical cell voltage because of the presence of activation polarization, concentration polarization, and ohmic polarization. Activation polarization is related to the charge transfer process involved in the electrochemical reactions. By making the electrode/electrolyte interfaces functionally diffuse, the region over which the charge transfer occurs can be enlarged, and the activation polarization can thus be considerably reduced. The concentration polarization is associated with the transport of both reactant and exhaust gases through the porous electrodes and is primarily governed by the microstructure of the electrode, specifically, the porosity, pore size, and pore geometry. The ohmic polarization arises from the resistance to the flow of ions in the electrolyte as well as resistance to the flow of electrons in the electrodes. Therefore, the useful voltage of an operating cell can be expressed as

$$E^0=E-IR_i-(\eta_a+\eta_c) \quad (1)$$

where E is open circuit voltage dictated by the operating temperature and type of fuel employed, IR_i is the ohmic polarization (I is the cell current, R_i is the internal resistance of cell encompassing the contributions of both electrolyte and electrodes), and η_a and η_c are the anode and cathode overpotentials, respectively. Overpotential at each electrode comprises activation and concentration polarizations. It is obvious from above formula that ohmic loss is a linear function of current providing the cell resistance remains essentially constant throughout the operation process. Activation polarization is a dominant loss mechanism at low level of current density. Concentration polarization occurs over an entire range of current density, but becomes prevalent at high current density where the supply of reactant species to the cell reaction sites becomes increasingly insufficient. Depending on the operating temperatures, the polarization losses usually account for 30%~60% voltage loss at peak power density. This is the primary reason why minimization of polarization losses has been a major goal in the research and development of SOFCs.

To accumulate the voltage output for practical applications, single cell is rarely utilized, instead, multiple cells are stacked in either electrical series or parallel or both where an interconnect is required for connecting the cells. Tubular and flat-plate stack designs are currently two most favored SOFC concepts under development (Minh, 1993; Singhal, 1999; Godfrey *et al*., 1999; Khandkar *et al*., 1999;

Kuroishi *et al*., 2001; Elangovan *et al*., 2001). Tubular design enjoys the status of the most advanced SOFC technology, and therefore holds the promise of first entering the stage of commercialization. It features the utilization of a thick and porous ceramic tube as support structure upon which cathode, electrolyte, anode, and interconnect are successively deposited. One salient feature of this design is that no seals are needed, hence issues associated with the gas-tight seals at elevated temperatures can be mitigated. Additionally, the individual cell is constructed as a fundamental unit structure that is subsequently connected in electrical series or parallel to enhance power-generating capacity. This allows the thermal stresses to be somewhat tolerated and concerns of thermal cracking to be greatly alleviated. However, due to the long current path along the plane of electrodes, the ohmic losses are unfavorably large. Moreover, since the ceramic support underneath the cathode is significantly thicker than the cathode itself, the oxidant must diffuse along a long pathway to reach the cathode/electrolyte interface to initiate the electrochemical reactions. This leads to the fact that the concentration polarization of the cathode constitutes the major portion of overall polarization losses (concentration polarization plus activation polarization). Both large ohmic losses and concentration polarization contribute to the less desired cell performance as well as the low power density characteristic of the tubular design. Besides, the highly complex and prohibitively costly fabrication and manufacture process inherent in this design is a dominant limiting factor for its mass production.

In comparison, the fabrication and stack assembly are much simpler for the flat-plate design where individual cell components are configured as thin, flat plates. This configuration provides considerable flexibility in the design of manifolds for transporting the gases in and out of the cells. It also offers the advantage of better quality control by evaluating the cell components individually. More importantly, flat-plate design demonstrates much improved cell performance and appreciably enhanced power density compared to the tubular one. This is largely attributed to the substantially reduced ohmic losses along the direction parallel to the thickness of the cell components. This design is amenable to a variety of processing techniques for making cell components. Some states-of-the-art techniques are capable of fabricating flat components on micrometer scale, offering the possibility of further reducing ohmic losses and lowering of operating temperatures. However, one distinct drawback of this type of design is that high temperature sealing is required to prevent the mixing of oxidant and fuel gases. Further, the nature of this design places stringent constraint on the thermal expansion match among cell components. Unacceptably large thermal stresses arising from the mismatch of thermal expansion coefficients can cause cracking and warping of the stack, leading to a rapid deterioration of SOFC performance. Regarding the flat-plate design, there is a growing trend in the SOFC community that electrolyte-supported configuration (where the electrolyte is the thickest component) is being increasingly replaced by anode-supported one (where the anode is the thickest component). The advent of anode-supported planar SOFC design, in principle, allows a ceramic interconnect to be replaced by a metallic interconnect due to the reduction of operating temperatures. Although the metallic interconnect was originally envisioned for electrolyte-supported planar SOFC, current interest in the development of metallic interconnects is mainly aimed at applications for anode-supported one. The present review is primarily concerned with the status of metallic interconnects by identifying some technical hurdles that must be addressed. The review is organized as follows: the roles of the interconnect in SOFC stack are first described, followed immediately by detailed explanations of demands for the interconnect to fulfil its required functions. Then outstanding issues in connection with the application of ceramics as interconnects are subsequently identified, and the shift toward the metallic interconnects in the SOFC community is rationalized in a separate section. The long-term oxidation behaviors of presently developed and some potential metallic interconnects are assessed with emphasis placed on promising alternatives to

extend their lifetime in SOFC environments. Closely associated with the oxidation performance of metallic interconnects is their contact resistance that is pivotal in determining their usefulness in practical SOFC stack. This topic is extensively covered and discussed in more detail. In tandem with the emergence of metallic interconnects is the intensive effort expended toward the development of viable coating materials as well as inexpensive coating techniques. This issue of critical importance is equally addressed in this review. Finally, the processing and fabrication of metallic interconnects directly related to their potential commercialization are dealt with.

ROLES OF INTERCONNECT IN SOFC STACK

As just mentioned, the interconnect in SOFC serves to multiply the voltage output by connecting individual cells in electrical series, which is schematically illustrated in Fig.2 for flat-plate design. In the anode-supported configuration, the interconnect serves also as a structural support since it is the bulkiest part among four components (anode, cathode, electrolyte, and interconnect). Note that, in comparison with single cell, two additional interfaces, i.e., interconnect/anode and interconnect/cathode, are introduced due to the incorporation of interconnect into the SOFC stack. In many circumstances, it is the unusually large contact resistance of these inter-phase boundaries that accounts for the greatly reduced power density of the stack as compared to the individual cell. Regardless of configurations, interconnect in essence physically separates yet electrically connects the anode of one cell to the cathode of the other. Specifically, it provides electrical connection between anode of one individual cell to the cathode of the neighboring one. It also acts as a physical barrier to protect the air electrode materials from being exposed to the reducing environment of the fuel on the fuel electrode side and prevents the fuel electrode materials from being attacked by the oxidizing atmosphere at the oxidant electrode side. Through the built-in ribs on both sides of the interconnect during fabrication, it commonly contains gas channels to provide fuel to the anode and oxidant to the cathode. Despite the fact that flow gas passages have also been built on the porous structure of the electrode layers, interconnect with built-in gas channels is preferred due to its cost-effective manufacture. The flat-plate design offers the advantage of multiple configurations of transporting gases in and out of the fuel cell. In the most common flow geometry, fuel flows in one face of the fuel cell stack and its reaction product flows out of the opposite face. Likewise, oxidant is introduced from one face of the fuel cell stack and its waste gases are removed from the opposite face. The gas channels on both sides of the interconnect can be constructed in the shape of either co-flow or counter-flow or cross-flow. Other conceived gas flow patterns include parallel flow and radial or axial flow with gas inlet and outlet situated inside the fuel cell stack.

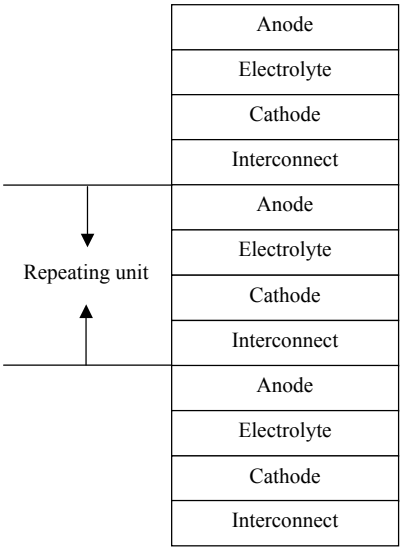

Fig.2 Schematics of stack of three individual fuel cells for flat SOFC design

REQUIREMENTS FOR SOFC INTERCONNECT

As the interconnect is required to serve multiple roles in the SOFC stack, the material requirements for the SOFC interconnect are the most demanding among all cell components. In particular, the chemical potential gradient arising from considerable oxygen partial pressure differences

between the oxidant and fuel places severe constraints on the choice of materials for the interconnect. In order to perform their intended functions, interconnects should have the following characteristics:

1. Under the SOFC operating temperatures and atmospheres (oxidizing at cathode and reducing at anode), interconnect must exhibit excellent electrical conductivity with preferably nearly 100% electronic conduction. This implies that not only the electronic transference number should be high, but also the absolute magnitude of the electrical conductivity should be reasonably large. Ideally, the ohmic loss generated as a result of the introduction of interconnects is so small that the power density of a stack does not suffer a prominent drop as compared to an individual cell. A value of 1 S/cm is a well-accepted minimum electrical conductivity for the usefulness of interconnects in SOFC community (Minh *et al*., 1990). This value is almost one to two orders of magnitude larger than the electrical conductivity of yttria-stabilized zirconia (YSZ) which is typically 0.1 S/cm at 1000 °C and 0.02 S/cm at 800 °C. YSZ is by far the most widely used solid electrolyte due to its excellent stability in both reducing and oxidizing atmospheres (Minh, 1993).

2. Interconnect should demonstrate adequate stability in terms of dimension, microstructure, chemistry, and phase at operating temperature around 800 °C in both reducing and oxidizing atmospheres, considering that they are exposed to oxidant on one side and fuel on the other. The oxygen partial pressure on the cathode ranges roughly from 10^{-4} to $10^{-0.7}$ atm, whereas on the anode side, it varies from 10^{-18} to 10^{-8} atm. Therefore, a significant oxygen partial pressure gradient builds up on two sides of interconnect. Any dimensional change in the presence of oxidizing and reducing atmospheres is likely to cause mechanical stresses whose magnitude may be large enough to initiate cracking or warping to the sealing, thus drastically degrading the overall stack performance. The microstructure of interconnect should remain relatively stable throughout the entire range of chemical potential gradient so that no appreciable variation of electrical conductivity develops during its expected lifetime service. From the viewpoint of environmental friendliness, the interconnect should ideally not contain any volatile species that subsequently react with possible contaminant gases such as H_2S, CO_2 in fuel. Phase transformation in the interconnect during operation inevitably accompanies sudden changes in its pertinent properties, and thus ought not to be allowed (Singhal, 2000).

3. It should have excellent imperviousness for oxygen and hydrogen to prevent direct combination of oxidant and fuel during fuel operation. This can be directly deduced from the following Nernst equation (Nernst, 1899) on the reaction of oxygen and hydrogen, that a slight decrease in the partial pressure of oxygen and hydrogen, resulting from the leakage of interconnects, may lead to a noticeable decline in the open circuit voltage (E) (Tde, 1989; Khandkar and Elangovan, 1991; Warde *et al*., 1976; Dollard and Brown, 1986; Maskalick, 1992).

$$E = E^{s} + \frac{RT}{2F}\ln\frac{P_{H_2}P_{O_2}^{1/2}}{P_{H_2O}} \tag{2}$$

where E^{s} stands for the ideal standard potential, R is gas constant, P gas pressure, T temperature, and F represents Faraday's constant. The drop in the open circuit voltage significantly reduces the electrical efficiency of the fuel cell. Cell efficiency is defined as the ratio between operating voltage and ideal voltage that is constant at the given condition (for instance, ideal voltage is 1.227 V at 25 °C, 1 atm for the reaction of pure hydrogen and oxygen gases to generate water product). It is apparent from Eq.(1) that a lower open circuit voltage leads to a lower operating voltage. For ceramic interconnects, the gas impermeability can only be achieved via full densification during fabrication. Moreover, the high density of the interconnect should be preserved throughout its service time (Singhal, 1999).

4. Regarding ambient and operating temperatures, the thermal expansion coefficient (TEC) of the interconnect should match well those of electrodes and electrolyte, so that the thermal stresses developed during stack startup and shutdown could be minimized. Since the YSZ electrolyte shows

TEC of around 10.5×10^{-6} per °C, the TEC of an interconnect should preferably be close to this value. This constraint is more stringent for ceramic interconnects than metallic ones as metallic materials are generally more compliant and flexible enough to somehow accommodate stresses compared to their ceramic counterpart (Minh, 1993). The degree to which the match of TECs among cell components should be achieved also depends upon the types of seals employed. If the seals are rigid (e.g. glass seals), thermal expansion match is of more importance. If the seals are flexible like compression seals, the requirement for expansion match can be somewhat relaxed.

5. No reaction or inter diffusion between interconnect and its adjoining components, specifically, anode and cathode, is allowed to occur under operation conditions. The desired chemical compatibility is of extreme importance and constitutes a challenging task for SOFC stack development given its considerably higher service temperature than other fuel cells. Any unexpected intermediate layers present at the boundaries of the interconnect and its neighbors tend to not only substantially increase ohmic loss, but also markedly promote polarization losses. As a consequence, the stability of the interconnect with respect to its contacting materials is vital for ensuring sustained desirable stack performance (Badwal, 2001).

6. The interconnect should possess fairly good thermal conductivity. Five W/(m·K) is considered to be an acceptable lower limit (Tsuneizumi, 1992). For application in the planar stack configuration, excellent thermal conductivity is highly desired and its advantage can be fully demonstrated. Interconnect with high thermal conductivity allows the heat generated at the cathode to be transported to the anode where the endothermic fuel reforming reaction takes place. This can greatly favor the replacement of external reforming with internal reforming. The immediate benefit will be a measurable cost decrease of the stack as a whole (Hirschenhofer *et al*., 1998).

7. Excellent oxidation, sulfidation and carburization resistances are requisite attributes for interconnect to qualify for application in SOFC-like environments. This does not pose any concern as long as perovskite-type complex ceramic oxides are utilized since the lattice diffusion coefficients of sulfur and carbon are negligibly small (Badwal, 2001). The issue does arise when metallic interconnects are considered because formation of metal oxide scales in SOFC gases is a thermodynamically favored inevitable process (Wright *et al*., 1997). Presence of sulfur and carbon-bearing gas species might aggravate the issue (Natesan, 1998). Comparatively, resistance to CO_2 and CO gas attack is of more significance since the sulfur-containing gases can be largely eliminated by prior desulfurization treatment.

8. The interconnect should be easy to fabricate, which is a key point in determining the feasibility of large-scale manufacture. The costs of raw materials as well as fabrication processes for the interconnect are also desired to be as low as possible so that they will not present major obstacles to commercialization. Cost reduction of interconnect is of particular significance for the anode-supported planar SOFC since it is the bulkiest part of all components.

9. The interconnect should also exhibit adequate strength and creep resistance at elevated temperatures. This requirement is of special relevance to the planar SOFC where the interconnect serves as a structural support.

CHARACTERISTICS OF CERAMIC INTERCONNECTS

Ceramic interconnects based upon complex ceramic oxides with perovskite structure have been subject of intensive study over the past several decades. It was found that only a few such oxide systems can fulfil the rigorous requirements for the interconnect materials in SOFC. Lanthanum chromite ($LaCrO_3$) is currently the most common candidate material since it demonstrates reasonably high electronic conductivity in both fuel and oxidant atmospheres, moderate stability in the fuel cell environments as well as fairly good compatibility with other cell components in terms of phase, mi-

crostructure and thermal expansion. In order to improve the electrical conductivity as well as modify the TEC, $LaCrO_3$ is often doped at lanthanum or chromium or both sites of the perovskite block unit for practical applications. Due to ionic radius similarity, strontium and calcium tend to replace La ions whereas magnesium, iron, nickel, copper and cobalt prefer to take over the site of Cr ions. As a matter of fact, in tubular SOFC configuration, doped $LaCrO_3$ is still the most widely used interconnect.

A considerable body of literature (Meadowcroft, 1973; Mizusaki *et al*., 1984; Karim and Aldred, 1979; Anderson *et al*., 1989; Flandermeyer *et al*., 1984; 1985a; Webb *et al*., 1977; Hofer and Kock, 1993; Yasuda and Hikita, 1993) addressed the nature of defect chemistry and electrical conductivity of doped $LaCrO_3$. It is now well-clarified that under high oxygen activity environment where oxygen partial pressure is typically larger than 10^{-8} atm, the charge imbalance due to the replacements of either La ion or Cr ion or both is electronically compensated by a $Cr^{3+}\rightarrow Cr^{4+}$ transition (Yasuda *et al*., 2001b; Park and Lee, 1997; Simner *et al*., 1999). This is also termed electronic compensation mechanism through which the occurrence of electron holes is promoted. On the other hand, under reducing atmosphere, the charge imbalance caused by the introduction of aliovalent dopants is achieved via the ionic compensation mechanism where the generation of oxygen vacancies is triggered. In the oxygen activity regime where both electronic and ionic compensation mechanism are operative, with the decrease in oxygen partial pressure, the lattice oxygen transforms into doubly charged oxygen vacancy of two electron holes simultaneously. This can be further illustrated by Fig.3 which shows variations of both electrical conductivity and oxygen vacancy concentration as a function of oxygen partial pressure for Mg-doped $LaCrO_3$ at two different doping levels at 1200 °C (Anderson *et al*., 1985). Above a critical oxygen partial pressure, the electrical conductivity is independent of oxygen partial pressure, indicating that only the electronic compensation mechanism is present. Increasing dopant content leads to the generation of a larger number of electron holes, thus promoting the electrical conductivity. As oxygen partial pressure falls off below the critical oxygen partial pressure, the electrical conductivity drops sharply, implying that the ionic compensation mechanism starts to be active (Boroomand *et al*., 1999; Flandermeyer *et al*., 1985b). Alternatively, the reduction in electron hole concentration contributes to the observed drastic drop in the electrical conductivity with decreasing oxygen partial pressure. This correlates well with the exponential increase of the oxygen vacancy concentration. More oxygen vacancies are induced at the expense of electron holes to compensate for the charge imbalance. The critical oxygen partial pressure at which a sudden drop in electrical conductivity occurs becomes lower as dopant concentration is reduced. It appears that improving electrical conductivity by means of raising dopant concentration can only be accomplished at relatively high oxygen partial pressure where electronic compensation mechanism is a prevailing player.

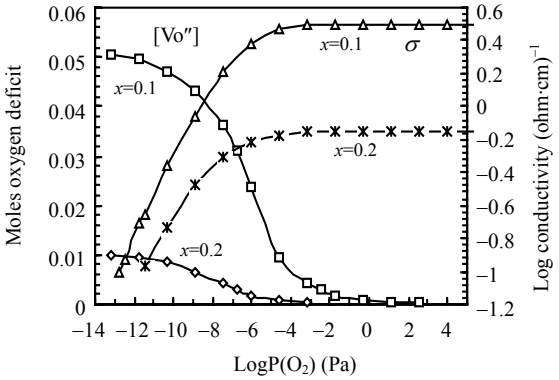

Fig.3 Oxygen vacancy concentration and electrical conductivity as a function of oxygen partial pressure and dopant content for $LaCr_{1-x}Mg_xO_3$ at 1200 °C (Anderson *et al.*, 1985)

Temperature also exerts pronounced influence on the electrical conductivity and its underlying dominant mechanism. Fig.4 plots the oxygen vacancy concentration and electrical conductivity as a function of oxygen partial pressure at two differing temperatures for $LaCr_{0.9}Mg_{0.1}O_{3-\delta}$. At sufficiently large oxygen partial pressure, the electrical conductivity shows little dependence on either tem-

perature or oxygen partial pressure (Anderson *et al*., 1985). This suggests that only electronic compensation occurs so that electron holes are being exclusively created. In other words, little or no oxygen vacancy is expected in such a highly oxidizing atmosphere. As the oxygen partial pressure is decreased below a critical value, the electrical conductivity drops exponentially. This is attributed to the sharp increase in the oxygen vacancy concentration, which indicates the onset of the ionic compensation mechanism. The critical oxygen partial pressure at which the ionic compensation mechanism is triggered decreases with decreasing temperature. Furthermore, at a fixed oxygen partial pressure where both electronic and ionic compensation mechanisms are active players, the electrical conductivity displays greater value at low temperatures than at high temperatures. This reveals that high temperature favors the formation of oxygen vacancies at the expense of electron holes. The profiles of oxygen concentration vacancy versus the oxygen partial pressure confirm the above interpretation. At extremely low oxygen partial pressure where the electroneutrality is solely maintained via the generation of oxygen vacancy, the oxygen vacancy concentrations are identical at two temperatures. Strong dependence of electrical conductivity on the oxygen partial pressure is one of the distinct characteristics of $LaCrO_3$-based ceramic interconnects.

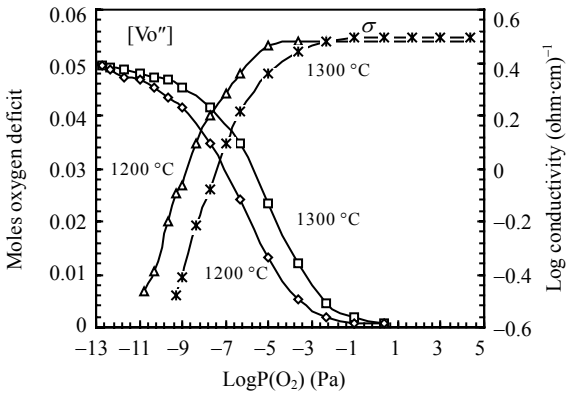

Fig.4 Oxygen vacancy concentration and electrical conductivity as a function of oxygen partial pressure and temperature for $LaCr_{0.9}Mg_{0.1}O_3$ (Anderson *et al.*, 1985)

The electronic conduction of doped $LaCrO_3$ ceramics is deemed to occur via the thermally activated hopping of small polarons. This evident in the plot of electricity conductivity of Sr-doped $LaCrO_3$ in air against temperature shown in Fig.5 of linear plots of Log(σT) vs $1/T$. The relationship between the electrical conductivity of this material type σ and temperature T, is established based on the following equation, expressive of typical p-type conductor behavior (Weber *et al*., 1987):

$$\sigma=(A/T)\exp(-E_a/kT) \quad (3)$$

where A is the pre-exponential factor, k the Boltzmann constant, and E_a the activation energy for conduction. It is evident from Fig.5 that higher doping level contributes to larger electrical conductivity, owing to the higher concentration of electron holes.

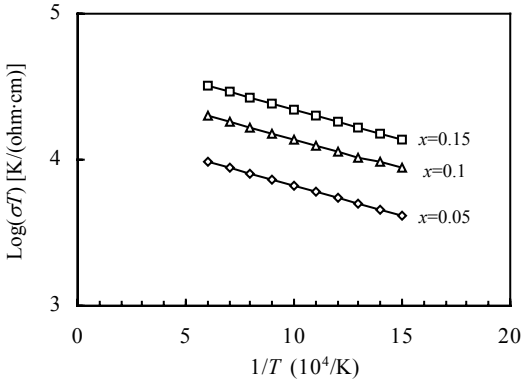

Fig.5 LogσT vs $1/T$ for $La_{1-x}Sr_xCrO_3$ ceramics (Weber *et al*., 1987)

Given a wide spectrum of oxygen partial pressures the interconnect is exposed to in SOFC environments, the implications for the dependence of the compensation mechanism on the oxygen partial pressure is of particular significance when doped $LaCrO_3$ is utilized as interconnect. Under oxidizing atmosphere such as oxygen or air at the cathode where the oxygen partial pressure is relatively high ($10^{-0.7}$ to 10^{-4} atm), conductivity is noticeably promoted due to the induced Cr^{3+} to Cr^{4+} transition via the electronic compensation mechanism. On the other hand, in reducing environments

such as fuel gases at the anode where the oxygen partial pressure is low (10^{-8} to 10^{-18} atm), the conductivity is considerably retarded because of the occurrence of oxygen vacancies via the ionic compensation mechanism (Meadowcroft, 1969). It naturally turns out that the electrical conductivity of the doped $LaCrO_3$ in reducing atmosphere like hydrogen is significantly lower than that in oxidizing atmosphere like air (Schmidt, 1981). Under such condition, a conductivity gradient across the doped $LaCrO_3$ is established that serves as an interconnect in the SOFC environments, considering that it is exposed to fuel on one side and oxidant on the other. Fortunately, the overall conductivity of the doped $LaCrO_3$ is still sufficient for that the operating temperature is above 800 °C (Minh and Takahashi, 1995). As the temperature drops below 800 °C, the electrical conductivity of the doped $LaCrO_3$ is reported to experience a substantial decline (Steele, 1994). This restriction renders it virtually useless for intermediate temperature SOFCs operating in the temperature range of 600~800 °C. This is also one of the reasons why the operating temperature of currently explored SOFC should be higher than 800 °C.

Study of their effects of many dopants incorporated into the $LaCrO_3$ ceramic on both TECs and electrical conductivities listed in Table 1 showed that: (1) cobalt doping significantly increases the electrical conductivity, unfortunately, the TEC also exhibits considerable increase (Tolochko *et al*., 1980; Tolochko and Kononyuk, 1986); (2) iron doping slightly improves the electrical conductivity while lowering TEC (Zhuk *et al*., 1988); (3) nickel doping results in a drastic increase in electronic conductivity and a transition to a metallic conductor typical for $LaNiO_{3-\delta}$, but, the stability and solid solution limit are considerably lower than cobalt and iron counterparts (Kononyuk *et al*., 1986); (4) magnesium doping enhances electrical conductivity,

Table 1 Thermal expansion coefficients and electrical conductivities of $LaCrO_3$-based solid solutions

Composition	Electrical conductivity (S/cm)	Composition	Average TEC ($\times10^{-6}$/°C)
$LaCrO_3$	0.34 at 700 °C, 1 at 1000 °C	$LaCrO_3$	9.5
$LaCr_{0.9}Mg_{0.1}O_3$	3 at 1000 °C	$LaCr_{0.9}Ni_{0.1}O_3$	10.1
$La_{0.9}Sr_{0.1}CrO_3$	14 at 1000 °C	$LaCr_{0.8}Ni_{0.2}O_3$	11.2
$La_{0.95}Ca_{0.05}CrO_3$	2.3 at 700 °C	$LaCr_{0.7}Ni_{0.3}O_3$	11.8
$La_{0.95}Ca_{0.05}Cr_{0.5}Co_{0.5}O_3$	63 at 700 °C	$LaCr_{0.9}Mg_{0.1}O_3$	9.5
$La_{0.8}Ca_{0.2}CrO_3$	7.1 at 700 °C, 35 at 1000 °C	$La_{0.9}Sr_{0.1}CrO_3$	10.7
$La_{0.8}Ca_{0.2}Cr_{0.8}Fe_{0.2}O_3$	9.2 at 700 °C	$La_{0.65}Ca_{0.35}CrO_3$	10.8
$La_{0.8}Ca_{0.2}Cr_{0.8}Ni_{0.2}O_3$	18 at 700 °C	$La_{0.8}Ca_{0.2}Cr_{0.9}Co_{0.1}O_3$	11.1
$La_{0.7}Ca_{0.3}CrO_3$	18 at 700 °C	$LaCr_{0.9}Co_{0.1}O_3$	13.1
$La_{0.7}Ca_{0.3}Cr_{0.8}Co_{0.2}O_3$	45 at 700 °C	$LaCr_{0.8}Co_{0.2}O_3$	14.6
$La_{0.7}Ca_{0.3}Cr_{0.5}Co_{0.5}O_3$	85 at 700 °C	$LaCr_{0.6}Co_{0.4}O_3$	18.7
$La_{0.7}Sr_{0.3}CrO_3$	15 at 700 °C	$LaCr_{0.2}Co_{0.8}O_3$	20.9
$La_{0.7}Sr_{0.3}Cr_{0.5}Co_{0.5}O_3$	58 at 700 °C	$La_{0.7}Sr_{0.3}Cr_{0.2}Co_{0.8}O_3$	19
$LaCr_{0.6}Ni_{0.4}O_3$	26 at 700 °C	$La_{0.7}Sr_{0.3}Cr_{0.5}Co_{0.5}O_3$	19
$La_{0.85}Sr_{0.15}CrO_3$	21.8 at 1000 °C	$La_{0.7}Sr_{0.3}Cr_{0.8}Co_{0.2}O_3$	14.5
$La_{0.87}Sr_{0.1}Cr_{0.95}Cu_{0.05}O_3$	23.9 at 1000 °C	$La_{0.87}Sr_{0.1}Cr_{0.95}Cu_{0.05}O_3$	9.81
$La_{0.85}Sr_{0.15}Cr_{0.98}Cu_{0.02}$	32.5 at 1000 °C	$La_{0.85}Sr_{0.15}Cr_{0.98}Cu_{0.02}O_3$	9.91
$La0_{.9}Sr_{0.1}Cr_{0.95}V_{0.05}O_3$	9.7 at 1000 °C	$La_{0.9}Sr_{0.1}Cr_{0.93}Mg_{0.05}Cu_{0.02}O_3$	9.61
$La_{0.85}Sr_{0.15}Cr_{0.95}V_{0.05}O_3$	19.9 at 1000 °C	$La_{0.9}Sr_{0.1}Cr_{0.95}V_{0.05}O_3$	9.87
$La_{0.9}Sr_{0.1}Cr_{0.9}Mg_{0.05}V_{0.05}O_3$	15.2 at 1000 °C	$La_{0.9}Sr_{0.1}Cr_{0.92}V_{0.05}Co_{0.03}O_3$	10.4
$La_{0.95}Sr_{0.05}Cr_{0.85}Mg_{0.1}V_{0.05}O_3$	12.9 at 1000 °C	$La_{0.85}Sr_{0.15}Cr_{0.95}V_{0.05}O_3$	10
$La_{0.87}Sr_{0.1}Cr_{0.935}Cu_{0.05}Co_{0.015}O_3$	25.6 at 1000 °C	$La_{0.9}Sr_{0.1}Cr_{0.9}Mg_{0.05}V_{0.05}O_3$	9.64
$La_{0.85}Sr_{0.15}Cr_{0.935}V_{0.05}Co_{0.015}O_3$	22.9 at 1000 °C	$La_{0.95}Sr_{0.05}Cr_{0.85}Mg_{0.1}V_{0.05}O_3$	9.22
$La_{0.9}Sr_{0.1}Cr_{0.92}V_{0.05}Co_{0.03}O_3$	12.8 at 1000 °C	$La_{0.87}Sr_{0.1}Cr_{0.935}Cu_{0.05}Co_{0.\ 015}O_3$	10.4
		$La_{0.85}Sr_{0.15}Cr_{0.935}V_{0.05}Co_{0.015}O_3$	10.5

while the TEC is hardly influenced (Anderson *et al*., 1978); (5) copper doping promotes both electrical conductivity and TEC (Armstrong *et al*., 1999); (6) strontium and calcium doping remarkably enhance electrical conductivity, while TEC is also considerably increased (Armstrong *et al*., 1995; 1996a; Srilomsak *et al*., 1989); (7) vanadium increases donor doping at the chromium site to reduce overall acceptor concentration. It is not surprising that both electrical conductivity and TEC decline as a result of vanadium doping (Armstrong *et al*., 1999); (8) double acceptor doping at both lanthanum and chromium sites generally brings about significant enhancement in electrical conductivity, but the concomitant increase in TEC is unfavorably large.

Some drawbacks inherent in doped $LaCrO_3$ exposed to reducing atmosphere deserve further attention. There exists so-called chemical coefficient of expansion that originates from the oxygen vacancy-triggered lattice expansion (Armstrong *et al*., 1995; 1996a; 1996b; Srilomsak *et al*., 1989; Hendriksen *et al*., 1995; Paulik *et al*., 1998; Hiei *et al*., 1999; Sakai *et al*., 1990a; Mori *et al*., 2000; Yakabe *et al*., 1999; Williford and Armstrong, 1999). As just described above, the concentration of oxygen vacancies is enhanced via the ionic compensation mechanism in reducing atmosphere. The observed lattice expansion with decreasing oxygen partial pressure shown in Fig.6 for acceptor doped $LaCrO_3$ and $YCrO_3$ is attributed to the increased cation size as Cr^{4+} transfers to Cr^{3+} ($R_{Cr^{3+}} > R_{Cr^{4+}}$) and/or increased cation-cation repulsion as bridging oxygen ions are removed (Armstrong *et al*., 1996b). The dramatic increase in the thermal expansion upon reduction of the oxygen partial pressure below a critical value marks the onset of the ionic compensation mechanism. At the same oxygen partial pressure, higher doping level leads to the creation of more oxygen partial pressure, and hence larger thermal expansion is expected. At the same doping level, Ca-doped $LaCrO_3$ expands more than Sr-doped $LaCrO_3$ does, due to the greater ionic size difference between Ca and La compared to that between Sr and La. This is one of the reasons why LSC is favored over LCC for interconnect applications. Doped $YCrO_3$ demonstrates much lower lattice expansion than doped $LaCrO_3$ when identical dopant is applied. Compositional optimization is imperative for minimizing isothermal expansion to avoid structural failure arising from the internal stresses developed during operation in SOFC environment. Besides, the acceptor-doped $LaCrO_3$ is more likely to have higher oxygen permeability in reducing gases as a result of significantly enhanced oxygen vacancy concentration. This gives rise to the promoted oxygen migration from the cathode to the anode via interconnect, which is responsible for the deteriorated fuel cell performance (Sakai *et al*., 2000). It has also been recognized that the mechanical properties of doped $LaCrO_3$ ceramics depend on the level of oxygen partial pressure, which constitutes another serious concern for their utilization as interconnects (Paulik and Armstrong, 2000; Meschke *et al*., 2000). Fig.7 clearly highlights the profound effect of oxygen partial pressure on the bending strength of Ca-doped $LaCrO_3$ and $YCrO_3$ (Paulik and Armstrong, 2000). In the region of relatively high oxygen activity, the doped chromites are capable of maintaining reasonable strength, but, as the oxygen partial pressure drops below 10^{-8} atm, the strength plummeted with decreasing oxygen partial pressure. Higher doping level results in greater decrease of strength. In comparison, Ca-doped $YCrO_3$ exhibits inherently lower strength than its lanthanum counterpart at high oxygen partial pressure with the strength deterioration occurring at much lower oxygen partial pressure.

One major obstacle to mass production of ceramic interconnects like $LaCrO_3$ or doped $LaCrO_3$ is their extremely inferior sintering behavior in air due to the easy volatilization of Cr (VI) species. The poor sinterability of $LaCrO_3$-based ceramics has been attributed primarily to the development of a thin layer of Cr_2O_3 at the interparticle neck at the initial stages of firing (Yokokawa *et al*., 1991). It was also noted that chromium evaporation resulting in chromium deficient composition impedes sintering. To achieve full densification, several options can be considered, although added manufacturing complexity and cost are inevitably incurred. The proposed approaches include (1) developing

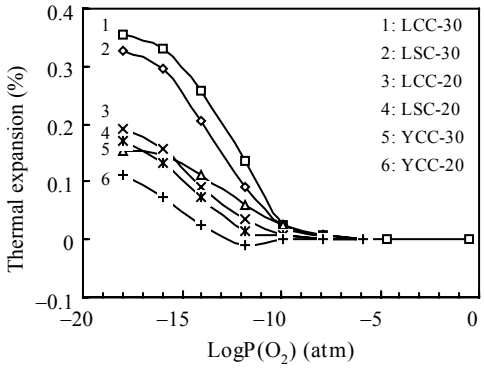

Fig.6 Expansion of acceptor substituted lanthanum and yttrium chromites at 1000 °C as a function of oxygen partial pressure (Armstrong *et al*., 1996b)

LCC-30 and LCC-20 refers to 30 mol% and 20 mol% Ca doped $LaCrO_3$, respectively. LSC-30 and LSC-20 represents 30 mol% and 20 mol% Sr doped $LaCrO_3$, respectively. YCC-30 and YCC-20 represents 30 mol% and 20 mol% Ca doped $YCrO_3$, respectively

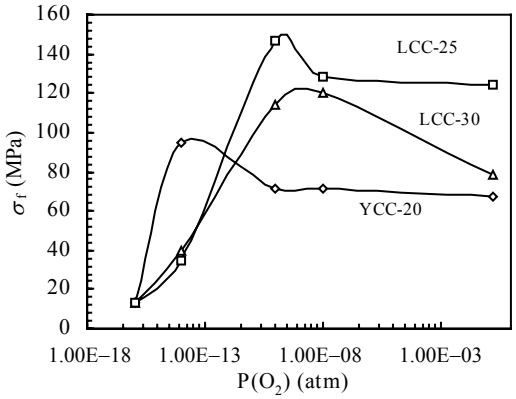

Fig.7 Room temperature bending strength of calcium substituted lanthanum and yttrium chromites as a function of $P(O_2)$ (Paulik and Armstrong, 2000)

LCC-25 and LCC-30 refers to 25 mol% and 30 mol% Ca doped $LaCrO_3$, YCC-20 represents 20 mol% Ca doped $YCrO_3$

new techniques to prepare highly reactive raw powders (Krogh *et al*., 1997; Chick *et al*., 1989), (2) conducting firing in reducing atmosphere followed by oxidation treatment to recover its high electrical conductivity, (3) adjusting the composition deliberately to facilitate the formation of non-stoichiometric perovskite structure (Sakai *et al*., 1990b; 1991; Bates, 1990; Mori *et al*., 1999), (4) conventional liquid-phase sintering process can be tried to promote densification (Flandermeyer *et al*., 1986), (5) firing $LaCrO_3$ between Cr_2O_3 plates (sandwich configuration) in conjunction with fast heating and cooling schedule to improve the densification process (Tai and Lessing, 1991).

DEVELOPMENT OF METALLIC INTERCONNECTS

To address the acute problems associated with ceramic interconnects, metal materials were initially envisaged to replace them as interconnects for electrolyte-supported planar SOFC. The invention of anode-supported planar SOFC design that has progressed considerably over the past several years is a major impetus behind the innovation in interconnect. The concept of an anode-supported SOFC, in principle, allows the doped $LaCrO_3$ interconnect to be replaced by a metallic one because of significant lowering of the operating temperature from 1000 °C to 800 °C. The use of 10~20 μm thick electrolyte in the anode-supported version leads to substantial reduction in the electrolyte ohmic polarization. In contrast, in the electrolyte-supported configuration, the electrolyte thickness is typically around 150 μm. A higher power density and a cost-effective fabrication process are claimed to be two main features of an anode-supported SOFC, and not surprisingly, this configuration is the focus of current study (Hsu, 1978; 1985). Recent work by Virkar (Virkar *et al*., 2000; Kim *et al*., 1999; Tanner *et al*., 1997) showed that, with the optimization of electrode structures to minimize both activation and concentration polarizations, a maximum power density in excess of 1.8 W/cm^2 can be achieved for an individual cell operating at 800 °C. Recent emergence of some viable techniques for the preparation of thin film electrolyte greatly accelerates the ultimate mass manufacture of this type of SOFC (Lindermann *et al*., 1995; Redd *et al*., 1996; Simwonis, 1997; Barthel *et al*., 2000; Chen *et al*., 2000; Okumura *et al*., 2000; Takenoiri *et al*., 2000; Tsukuda *et al*., 2000).

Table 2 compares ceramic interconnects with metallic ones. Obviously, there are many advantages in preparing the interconnect from a metallic

Table 2 Comparison of metallic and doped $LaCrO_3$ interconnects

Property	Metallic interconnect	Doped $LaCrO_3$ interconnect
Electrical conductivity	n-type electronic conductor	p-type electronic conductor
	Charge carrier: electron	Charge carrier: hole
	Conduction mechanism: electron hopping $\sigma=A\exp(E_a/kT)$ (<1100 °C)	Conduction mechanism: small polaron hopping $\sigma T=A\exp(E_a/kT)$ (<1100 °C)
	Conductivity: very high	Conductivity: sufficient for use at operating temperature >800 °C
	Ohmic losses are the least among SOFC components and can be neglected	Ohmic losses are much larger than those of electrodes, but smaller than that of electrolyte, cannot be neglected
	Suitable for both intermediate and high temperature SOFC	Only suitable for high temperature SOFC
Thermal conductivity	High	Low
	Heat can transport from air electrode to fuel electrode where endothermic reforming reaction occurs (allows for internal reforming)	Cooling fluid (normally excess air) is required at air electrode
Thermal expansion coefficient (from 25 to 800 °C)	Generally larger than that of ZrO_2 (8 mole% Y_2O_3) electrolyte, vary considerably from Cr-based to Ni-based alloys	Comparable to that of ZrO_2 (8 mole% Y_2O_3) electrolyte
Chemical stability	Spontaneous oxidation in atmosphere of high oxygen partial pressure, fairly good sulfidation and carburization resistance	Evaporation of Cr in oxidizing atmosphere (Cr^{3+} to Cr^{6+}), contaminant tolerance is low, Cr^{6+} (g) reacts with H_2S, CO_2 to form CrS_3 and Cr_2C_3
Dimensional stability	Stable	Lattice expansion in reducing atmosphere
Microstructural stability	stable	The number of electrons is increased in oxidizing atmosphere due to the transition of Cr^{3+} to Cr^{4+} via electronic compensation mechanism, appearance of oxygen vacancies in reducing atmosphere via ionic compensation mechanism, electrical conductivity gradient occurs
Reactivity with other SOFC components	No reactions between interconnect and adjacent components reported	Reaction with cathode after long-term service to form spinel phase due to the volatilization of Cr species
Mechanical integrity	No effect of oxidizing and reducing atmosphere on mechanical properties, mechanical strength at elevated temperatures is drastically lowered compared to room temperature, incorporation of oxide dispersoids improves high temperature mechanical properties	Degradation of mechanical properties in reducing atmosphere
Contact resistance	May be unacceptably large due to the development of insulating oxide scale on surfaces	No issue of contact resistance
	Coating is required in application	No coating is required

Permeability	Impervious to reactant gases	High oxygen diffusivity in reducing atmosphere leading to enhanced oxygen transport through interconnect from cathode to anode, deteriorating the fuel cell performance
Fabrication approach	Melt metallurgy Powder metallurgy Tape casting	Tape casting Powder sintering (hot pressing or hot isostatic pressing) Electrochemical vapor deposition
Sinterability	Full densification is readily achieved via melt or powder metallurgy	Very difficult to sinter, additional measures must be taken, manufacturing complexity and added cost are ensued
Workability	Excellent (ductility)	Poor (brittle)
Cost of raw materials	Low	Very high
Impact on environment	No pollution	Environmentally hazardous

material instead of a ceramic material. Since the electrical conductivity of metallic materials is realized via the migration of valence electrons, their electrical conductivities are generally several orders of magnitude larger than those of acceptor-doped $LaCrO_3$ ceramics. Hence, the ohmic losses in the metallic interconnect are small enough to be neglected. More importantly, unlike the ceramic interconnect, the electrical conductivity of metallic interconnect is independent of oxygen partial pressure that typical stretches over a wide range for SOFC. In particular, metallic interconnect is favored over the ceramic one because of their low cost, easy manufacture, and good workability. It should be reiterated here that the low cost of raw materials and fabrication process characteristic of the metallic materials are of prominent significance, considering that the interconnect in the anode-supported design is the bulkiest item in the SOFC, and thus is the major part of the total cost of the interconnect. In addition to the desired electrical conductivity, the excellent heat conduction unique to metallic materials, facilitates the easy transport of heat generated at the air electrode to the fuel electrode where the endothermal reforming reaction takes place (internal reforming) and dispenses with the use of cooling fluid that is usually excess air at the cathode (Tiffee *et al*., 1990). Another good feature of the metallic interconnect is that it offers the possibility of flexible design. For instance, the envisioned window-frame design allows the use of relatively small area of electrolyte-electrode structures that are in contact with the large metallic bipolar plate. More advantageously, this design featuring the buildup of parallel gas grooves shows less electrical resistance than the dimple design where the multiple gas manifolds are constructed perpendicular to the major plane of the flat SOFC. This presumably arises from the larger contact area between interconnect and adjoining electrodes for the dimple design as compared to the window-frame design.

The most prominent issues associated with the use of metals as interconnects for SOFC include the lack of adequate mechanical strength at operating temperatures, poor oxidation, sulfidation, and carburization resistance in service environments, as well as unfavorably larger thermal expansion coefficient of metallic interconnect than those of its contacting components. It is well known that mechanical properties of the metallic materials decline sharply with increasing temperature, although this problem has been greatly alleviated via some proved successful means such as refining of grain size, incorporation of oxides of oxygen reactive elements, or a combination of both. As will be elaborated later, the incorporation of nanosize oxides is of particular benefit since it can also significantly improve the oxidation resistance and integrity of the oxide scale of many alloys exposed to oxidizing atmosphere. Especially noteworthy among the required attributes for metallic inter-

connects, perhaps the most stringent, is the excellent oxidation resistance. Considering that an oxide layer inevitably develops on the surface of metals exposed for a long time to oxidizing environment, it is imperative that the prospective metallic interconnects display exceptionally slow growth of scale over the projected service lifetime (40000 h) of the SOFC. Most importantly, the oxide scale formed should exhibit sufficiently high electronic conductivity so that the ohmic losses do not constitute a major source of stack performance degradation. The oxides should also be chemically stable, dense, free of defects, and strongly adhered to the metal on the scale/substrate interface. Another technical problem to be handled is the thermal expansion mismatch between metallic interconnect and the rest of the ceramic SOFC components. In particular, when it comes to the rapid heating and cooling frequently encountered in such applications as auxiliary power unit for automotive and portable power sources for laptops, the requirement for thermal compatibility is more rigorous. As metallic materials usually have inherently higher thermal expansion coefficients than ceramic ones, any measure to reduce the thermal expansion and shrinkage from the alloy design standpoint is acceptable provided that other critical properties are not compromised. Also, there is a growing trend to replace the rigid seal used in ceramic interconnects with compression flexible seal to accommodate more thermal stresses confronted in the SOFC stack with metallic interconnects. All the above problems of metallic interconnect are due to the high operating temperature of the SOFC, and can be partially or entirely mitigated by lowering its working temperature. Therefore, in parallel with the attempt to replace $LaCrO_3$ with metal, there is also a concerted effort to reduce the operating temperatures of SOFC, preferably to between 600 °C and 800 °C. Admittedly, the challenges to maintain the same power densities as those at elevated temperatures are tremendous.

Currently, there are no commercially available alloys that fulfil all the criteria to be viable interconnects for SOFC. Most research efforts have primarily focused on the Cr-forming alloys. Most recently, we developed metallic interconnects based on aluminide alloys and examined their viability in SOFC environments. In what follows, the benefits and limitations of these alloys from the perspectives of oxidation and thermal expansion behavior are described. The status of contact resistance of these alloys exposed to oxidizing atmosphere is discussed separately in the next section.

Chromium-based alloys

Chromium-based alloys were initially developed as a replacement of ceramic interconnects for electrolyte-supported planar SOFC. They are favored because of their moderate oxidation resistance and fairly good corrosion resistance provided by the formation of Cr_2O_3 scale in the presence of oxidant. In addition, the binary metal oxide Cr_2O_3 has comparatively large electronic conductivity (Samsonovin, 1973). Moreover, the thermal expansion behaviors of these alloys in the temperature range of 25 °C to 1000 °C, as indicated in Fig.8, exhibit considerable resemblance to that of ceramic component like YSZ (Quadakkers *et al*., 1994). Obviously, Cr-0.4La_2O_3 and Cr-5Fe-1Y_2O_3 alloys demonstrate thermal expansion response like that of YSZ. As a matter of fact, Cr-5Fe-1Y_2O_3 alloy was intentionally developed to match the TECs of other ceramic components in planar SOFC. The decreased TEC mismatch contributes favorably to the reduction of thermal stresses caused by rapid heating and cooling processes.

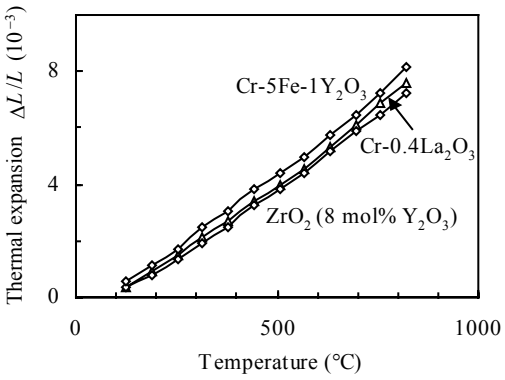

Fig.8 Comparison of thermal expansion of chromium-based alloys with that of ZrO_2 (8 mol% Y_2O_3) electrolyte (Quadakkers *et al*., 1994)

The major drawback of chromium-based alloys as metallic interconnects is their unacceptably high oxidation rate. The advantage of large electronic conductivity of Cr_2O_3, however, is in part offset by its rapid growth rate which is usually four orders of magnitude larger than that of Al_2O_3. In particular, the diffusivity of Cr is more significantly promoted than that of Al at temperatures higher than 700 °C.

It should be reiterated that an enhancement in the electrical conductivity and a drop in the growth rate of the oxide scale are contradicting goals so an acceptable compromise should be sought. One effective and straightforward approach to promote the oxidation resistance and adherence of scale to the metallic substrate involves the incorporation of the oxides of reactive elements like Y and La. The addition of these oxide dispersoids is well documented to improve the oxidation resistance by retarding the kinetics of the scaling process. The grain size of the oxide layer is also reported to be refined via the dragging mechanism due to the presence of the exotic additives (Quadakkers *et al*., 1994; Kofstad, 1996). More favorably, the integrity of the scale can be substantially strengthened owing to the greatly suppressed scale spallation tendency caused by the added oxides. Fig.9 shows the corrosion behavior of Cr-5Fe-1Y_2O_3 (in weight percentage) and Cr_3Co alloys exposed to varying atmospheres. By comparison, the role of yttria is rather pronounced. Significant mass gain is observed for Cr_3Co alloy exposed to air at 950 °C, when the scale starts to spall off after 1500 h exposure, as indicated by the weight loss. In contrast, the mass gain of the Y_2O_3-bearing alloy after being exposed to air is sharply reduced, and scale delamination is virtually eliminated. Of particular relevance to SOFC application is the observation that the scale grows faster in the presence of water plus hydrogen than in the presence of pure air for chromium-based alloys, since the humidified hydrogen is a preferred fuel gas for accelerating the kinetics of the electrochemical reaction. It was also noted that the addition of CO into the fuel atmosphere worsens the corrosion process, thus leading to more noticeable weight gain. Another attendant benefit for the interconnect resulting from the Y_2O_3 addition application is the improved mechanical properties at elevated temperatures as evidenced by Cr-5Fe-1Y_2O_3 alloy compared to pure chromium alloy. The direction of mass transport in the chromia scales is found to be predominantly outward chromium diffusion for alloys without oxides as opposed to mainly inward oxygen diffusion for alloys containing oxide additives. The morphology of the growing Cr scales is also improved by the presence of oxide dispersoids as these scales have fewer cavities, are denser, and more homogeneously distributed. The underlying mechanism is revealed to be the segregation of these oxides to the grain boundaries of the chromia scales (Bredesen and Kofstad, 1996).

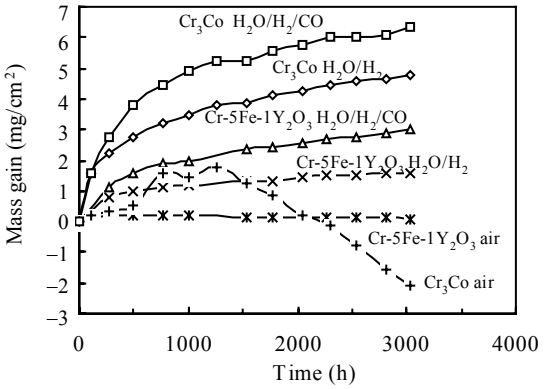

Fig.9 Corrosion response of Cr_3Co and Cr-5Fe-1Y_2O_3 alloys at 950 °C in different atmospheres (Quadakkers *et al*., 2000; Ueda and Taimatsu, 2000)

Although the envisaged chromium-based alloys typical of Cr-5Fe-1Y_2O_3 are originally intended to be replacements for ceramic interconnects of electrolyte-supported planar SOFC, their long-term oxidation performance at operating temperatures is still far from satisfactory. Despite the incorporation of oxides of reactive elements, the growth rate of the scale above 800 °C is excessively large. For instance, the oxide scale thickness on Cr-5Fe-1Y_2O_3 alloy is estimated to be around 10 μm after 1 year and 23 μm after 5 years operation at 900 °C. Such layer is considered to be too thick for reliable operation (Kofstad, 1996).

One of the distinctive problems with the chromium-based alloys, and in general, all

chromia-forming alloys, has been identified to be the formation of volatile gaseous Cr (VI) species at the fuel cell operating temperatures (Urbanek *et al*., 2000; Dulieu *et al*., 1998). These high valence Cr species such as CrO_3 (g) and $Cr(OH)_2O_2$ (g) develop literally simultaneously with the formation of Cr_2O_3 scale at the cathode side of the interconnect. Further oxidation of Cr_2O_3 scale usually takes place at the higher oxygen partial pressure end of the cathode prior to the electrochemical reduction of oxygen. Due to their unusually large vapor pressures, these species have been shown to diffuse into and interact with the $LaMnO_3$ based air electrodes, leading to a change in the air electrode composition and formation of new phases such as the $(CrMn)_3O_4$ spinel (Dulieu *et al*., 1998). The electrochemical performance of SOFCs is severely damaged due to the generation of volatile Cr species at the cathode of the fuel cell. Additionally, these species can interfere adversely with the oxygen reduction reaction by taking up electrons at the cathode, especially at the low end of oxygen partial pressure, resulting in the deposition of Cr_2O_3 at the electrode/electrolyte interface. The deposition of Cr_2O_3 has been revealed to proceed via one of the following reactions, depending on the specific type of Cr species (Hilpert *et al*., 1996; Badwal *et al*., 1997) (For the sake of understanding, the electrochemical reactions occurring at the cathode and anode, using oxygen as oxidant and hydrogen as fuel, can be written respectively as: $O_2+2e=O^{2-}$; $H_2+O^{2-}=H_2O+2e$):

$$2CrO_3\ (g)+6e=Cr_2O_3+3O^{2-} \quad (4)$$

$$2Cr(OH)_2O_2\ (g)+6e=Cr_2O_3+2H_2O+3O^{2-} \quad (5)$$

The reduction of volatile species to the solid Cr_2O_3 at the cathode/electrolyte interface constitutes another major cause for the rapid performance deterioration of the cathode as observed in the case of Cr-5Fe-1Y_2O_3 metallic interconnect. The underlying factors of the performance degradation are determined to be the diminished three phases (electrode/electrolyte/gas) area, suppressed surface electrochemistry of the cathode, and reduced active sites for the oxygen reduction reaction (Batawi *et al*., 1996).

Iron-based alloys

Iron-based alloys have some apparent advantages over chromium-based ones in terms of high ductility, easy machinability and low cost. Since the currently developed iron-based interconnects contain at least 17 wt% Cr, the role of which is to beep formation of corrosion-resistant Cr_2O_3 scale, the issue of cathode contamination by volatile chromium species encountered in the chromium-based interconnects also occurs. The mass gain as a function of time for various Fe-Cr-based alloys exposed to air at 800 °C is presented in Fig.10 (Quadakkers *et al*., 2000). It was found that in the case of Fe-17Cr-0.4Y-2Ni, addition of nickel virtually eliminates the chromia scale despite the presence of reactive elements, and hence causes a significant weight gain after exposure for less than 100 h. For Fe-Cr alloys containing neither reactive nor alloying element, the growth rate of the oxide scale is exceedingly high, effectively making these alloys useless for interconnect application. Incorporation of Mo moderately suppresses the growth kinetics of Cr_2O_3 scale as illustrated by the oxidation behavior of Fe-26Cr-1Mo alloy. Apparently, the weight gain is still too large for the alloy to qualify as SOFC interconnect. Addition of either Ti or Mn promotes the oxidation rate, which explains the unusually large mass gain observed for the Ti- or Mn-bearing alloys. It is noteworthy that manganese addition is designed to develop surface scales comprising the spinel Cr_2MnO_4 or a spinel layer on the top of an inner Cr_2O_3 layer. Although the overall thickness of surface scales is increased, the electrical resistance can be discernibly lowered, which is attributed to the relatively low electrical resistivity of Cr/Mn-spinel phase involved. Advantageously, incorporation of oxygen-reactive elements such as Y can significantly retard the oxidation kinetics of iron-based alloys. This can account for the least weight gains obtained for Fe-25Cr-0.2Y and Fe-16Cr-0.2Y alloys even after exposure at 800 °C for up to 1000 h. Therefore, like the chromium-based alloys, presence of reactive elements, though in trace amounts, is equally beneficial in providing desired oxidation resistance to the iron-based alloys. However, it is premature to

recommend the above two alloys as prospective interconnect candidates since other pertinent parameters such as the thermal expansion coefficients and contact resistance of the alloys exposed to SOFC environments for long time are currently unavailable.

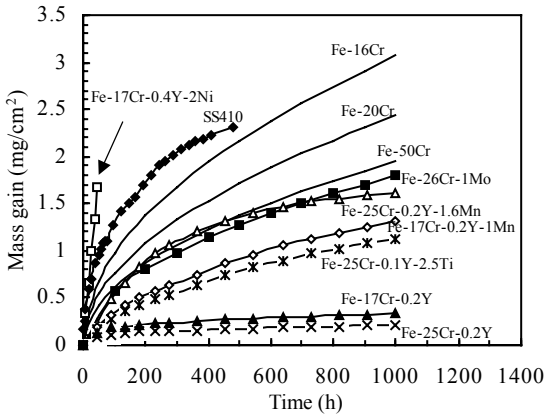

Fig.10 Oxidation behavior of various Fe-Cr-based alloys at 800 °C in air (Montealegre *et al*., 2001)

Thermal expansion characteristics of some iron-based alloys examined for possible utilization as interconnect materials are given in Fig.11 (Quadakkers *et al*., 2000; Ueda and Taimatsu, 2000). For comparison, thermal expansion behaviors of ZrO_2 (8 mol% Y_2O_3) electrolyte and Sr-doped $LaCrO_3$ ceramics are also presented. All alloys display larger thermal expansion than YSZ electrolyte to varying degrees. Addition of nickel into the Fe-18Cr alloy substantially promotes the thermal expansion, while tungsten addition into the same matrix alloy considerably suppresses the thermal expansion. Fe-26Cr-1Mo and Fe-18Cr alloys exhibit comparable thermal expansion behavior at temperatures below 800 °C, implying that Cr and Mo play opposite roles in affecting the thermal expansion of pure iron. The thermal expansion of Inconel X-750 upon heating to 1000 °C is somewhere between those of Fe-18Cr-8Ni and Fe-18Cr alloys. It appears that, to satisfy the requirement of thermal match among SOFC components, Fe-18Cr-9W alloy is a promising metallic interconnect as its thermal expansion coefficient is the closest to that of YSZ electrolyte. Further studies on the oxidation performance at 800 °C in SOFC atmospheres for extended time, in particular, the contact resistance of the alloy subjected to long-term oxidation must be studied and known in order to achieve a meaningful assessment of its applicability as interconnect.

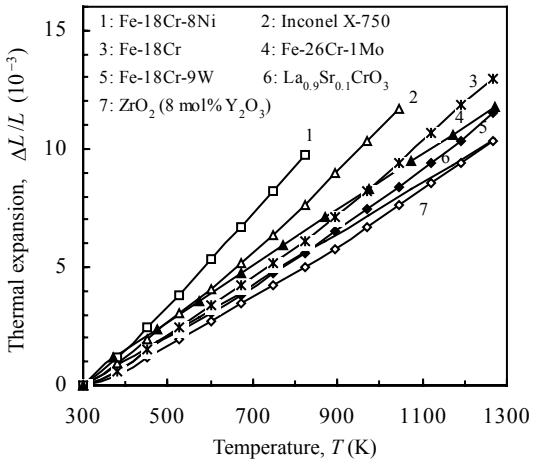

Fig.11 Comparison of thermal expansion of some Fe-Cr-based alloys with that of ZrO_2 (8 mol% Y_2O_3) electrolyte (Quadakkers *et al.*, 2000; Ueda and Taimatsu, 2000)

Thermal expansion characteristic of $La_{0.9}Sr_{0.1}CrO_3$ is also given for comparison

Nickel-based alloys

Nickel-based alloys have been evaluated for their suitability as metallic interconnects in both fuel and oxidant atmospheres. These alloys are resistant to high temperature and typically include nickel, chromium, iron and manganese. They are also attractive because of their slower oxidation kinetics than their stainless steel counterparts. The apparent disadvantage in their application as interconnect is their larger thermal expansion coefficients as compared to iron-based alloys. To remedy this, the proposed interconnect constructed of this type of alloy is preferably in the form of a thick foil that is typically around 0.1 mm. Obviously, gas channels interconnecting the oxidant and fuels must be incorporated into the cathode and anode, respectively. On the other hand, the enhanced deformability inherent in nickel-based alloys in relation to the iron-based ones, and the flexibility of a metallic foil allow for the accommodation of strain caused by the mismatch in the thermal expansion coefficients

of the mating parts. England and Virkar (1999; 2001) examined oxidation behaviors of four types of commercially available alloys, i.e., Inconel 625, Inconel 718, Hastelloy X, and Haynes 230 in both air and wet hydrogen. Their results are presented in Fig.12 showing that oxidation event takes place not only in air but also in wet hydrogen where the partial oxygen pressure is relatively low. Moreover, the oxidation kinetics in wet hydrogen are faster than that in air. Since chromia is identified as the dominant oxide phase formed in all the alloys examined, the above results indicate that chromia is a thermodynamically stable phase throughout the entire range of oxygen partial pressure in the fuel cell. The slower oxidation rate of Haynes 230 as compared to the other three alloys studied may be due to the formation of a two-phase composite oxide ($Mn_{1+\delta}Cr_{2-\delta}O_{4-\lambda}$ and Cr_2O_3) scale and/or the nature of the oxide defect chemistry. As will be described latter, it appears that the presence of manganese in adequate amounts in nickel-based alloys not only effectively reduces oxidation resistance, but considerably reduces the contact resistance as well.

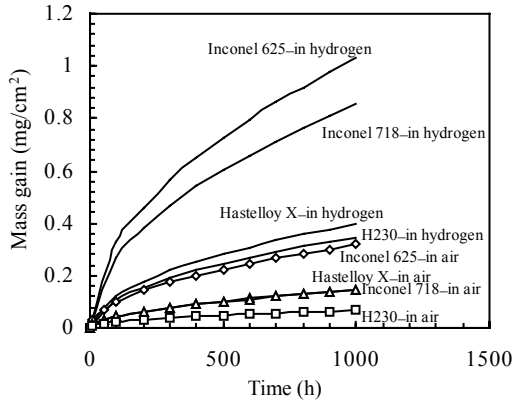

Fig.12 Oxidation behaviors of four Ni-based superalloys considered as possible interconnects during their exposure to two kinds of atmosphere at 800 °C. Note that alloys exposed to humidified hydrogen exhibit significantly larger mass gain than exposed to air (England and Virkar, 1999; 2001)

Aluminide alloys

Alumindes have been extensively investigated for structural applications at elevated temperatures because of their unique combination of high strength, reasonable ductility, and light weight. The SOFC interconnect simultaneously serves as a structural and functional unit in the stack at operating temperatures. Aluminides might be promising candidates for this specific application. Therefore, we assessed the suitability of aluminide alloys as interconnects for SOFC operating at temperatures ranging from 600 °C to 800 °C, in terms of oxidation resistance and thermal expansion behavior (Zhu and Deevi, 2003). The driving force behind the study is that with the emergence of the innovative technology of anode-supported planar SOFC, the operating temperatures can be decreased below 800 °C. Thus, the formation of a contagious insulating alumina scale might be avoided as these alloys are exposed to SOFC-like environments. Presumably, a mixture of metastable alumina and other transient oxides on the surface of oxidized alloys still provides desired oxidation, carbonization, and sulfidation resistance while maintaining reasonably low electrical resistivity. Oxidation behaviors of five compositions of iron and nickel aluminides were examined at 800 °C in air for 1000 h. The experimental results are shown in Fig.13. For comparison, the mass gain as a function of exposure time for iron-based stainless steel SS410 was concurrently measured and is shown in the same figure. As expected, iron aluminides showed greater oxidation resistance than do SS410 and nickel aluminide (Ni_3Al). With regard to iron aluminides, partial substitution of chromium for aluminum influenced little their oxidation performance. The scales formed exhibit fairly good integrity as no delamination or spallation was observed. Results of phase identification of scales using XRD after 1000 h oxidation indicate that preponderance of phases formed are transient oxides or nitrides like Fe_2O_3, NiO, Fe_4N, and AlN along with minor amounts of Al_2O_3. Since the oxidation rate of NiO is well recognized to be significantly larger than those of Fe_2O_3, Cr_2O_3, and nitrides, it is not surprising that Ni_3Al shows much more weight gain than do aluminide and Fe-based alloys after prolonged exposure to air at 800 °C. Experiments seemed to show that iron aluminides are favored

over nickel alumides for use as metallic interconnects due to their lower oxidation resistance. Further tests on the oxidation response of iron aluminides in both oxidizing and reducing atmospheres over even longer periods of time are necessary to gain deeper insight into their potential as interconnects.

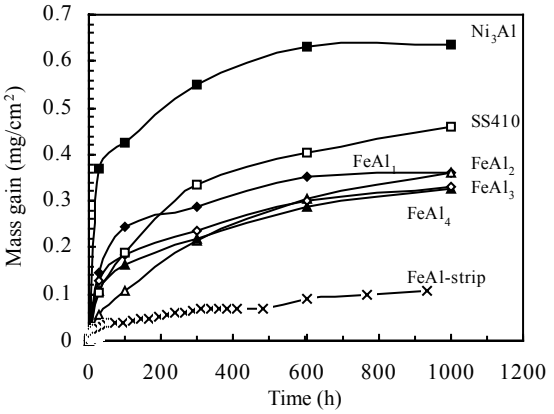

Fig.13 Mass gain as a function of time for some iron and nickel aluminide alloys exposed to air. The compositions of the alloys: examined are (in weight percent) (Zhu and Deevi, 2003)

FeAl-strip: Fe-24Al-0.42Mo-0.05B-0.08C,
$FeAl_1$: Fe-25Al-0.42Mo-0.1Zr-0.05B-0.08C,
$FeAl_2$: Fe-24Al-0.42Mo-0.1Zr-0.05B-0.08C,
$FeAl_3$: Fe-12Al-6Cr-0.42Mo-0.1Zr-0.05B-0.08C,
$FeAl_4$: Fe-18Al-6Cr-0.42Mo-0.1Zr-0.05B-0.08C,
Ni_3Al: Ni-8.1Al-5.23Cr-7.02Mo-0.13Zr-0.005B

For the metallic alloys to be competitive as promising interconnects for SOFC, their thermal expansion behaviors ought to resemble that of electrolyte to prevent stress-induced cracking or even disintegration of the whole stack. Although this requirement on the metallic interconnects can be more or less relaxed, depending on the sealing material adopted, as compared to the ceramic ones due to their greater ability to accommodate elastic deformation, alloys exhibiting thermal expansion coefficient similar to that of electrolyte (between ambient temperature and 800 °C) is almost always preferred. Fig.14 depicts the thermal expansion versus temperature for iron and nickel aluminide alloys and SS410 (Zhu and Deevi, 2003). Also depicted is how much yttria-stabilized zirconia (YSZ), the most commonly used solid electrolyte, expands as it is heated above 800 °C. Among all compositions studied, alloy Fe-12 wt% Al-6 wt% Cr-0.42 wt% Mo-0.1 wt% Zr-0.005 wt% B-0.08 wt% C was observed to have thermal expansion behavior closest to that of YSZ. It turns out that increasing either Fe or Al or Ni elemental content promotes thermal expansion with Al showing the most significant effect. Another conclusion derived from this study is the preclusion of SS410 as a prospective interconnect material on account of the sudden lattice shrinkage as it undergoes ferrite to austenite phase transformation at around 800 °C.

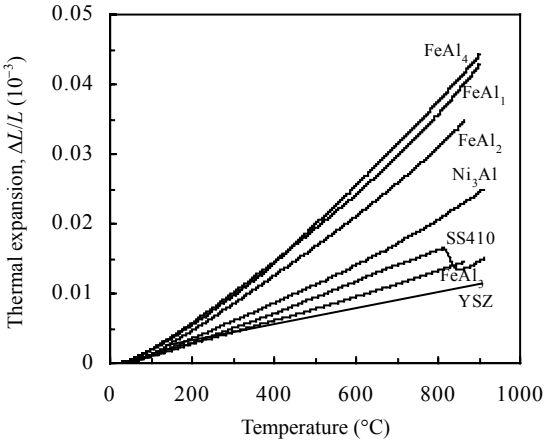

Fig.14 Thermal expansion response of various iron and nickel aluminide alloys (Zhu and Deevi, 2003)

CONTACT RESISTANCE OF METALLIC INTERCONNECTS

It is understandable that metallic interconnects are in principle preferred over ceramic interconnects since their bulk electrical resistivities are usually several orders of magnitude smaller. However, one of the major concerns that is associated with the use of metallic interconnects is the development of a semi-conducting, or even insulating, oxide scale during their extended exposure to SOFC-like environment. The contact resistances between an interconnect and its neighboring components become so dominant that the electrical efficiency of the stack drops sharply, despite a fairly high efficiency of the individual cells. As a result, stable operation of a SOFC stack can be

difficult to sustain at a working current density. Minimizing the contact resistance is vital to the development of competitive metallic interconnects, and holds the key to the successful commercialization of the anode-supported planar SOFC stack design for a variety of applications in the power industry.

Theoretical consideration

Since a layer of protective oxide scale inevitably develops on a metal surface in an oxidizing environment at elevated temperatures, the ultimate commercialization of metallic interconnects depends, to a large extent, on success fully dealing with the increase in the contact resistance due to the formation of the oxide layer. The large contact resistance of metallic interconnects is a major concern due to the drastic drop of the electrical efficiency and premature failure of the stack over the projected service lifetime (40000 h). In this particular application, requirements for the oxide scale are: (1) the oxide growth rate of oxide in both cathodic (air) and anodic (fuel gas plus water vapor) atmospheres should be as sluggish as possible; (2) the oxide scale should be strongly adhered to the alloy substrate to withstand thermal cycling without any spallation or delamination; (3) the oxide scale should be homogeneous in microstructure and uniform in thickness, be free of porosity or anomalous grain growth; and (4) the oxide scale should be a good electrical conductor at the operating temperature.

The contact resistance of an oxidized metallic interconnect is usually characterized by the area specific resistance (ASR), which is the product of electrical resistivity of the studied layer and its thickness. The acceptable ASR level for the metallic interconnect during service is generally considered to be below 0.1 $\Omega\cdot cm^2$. For alloys that have been exposed to air at the operating temperature of SOFC, e.g. 800 °C, for a period of time, oxide scale forms on both sides of the sample. The ASR of such an oxidized alloy can be expressed as:

$$ASR=\tau_s l_s+2\tau_o l_o \tag{6}$$

where τ_s and l_s are the resistivity and thickness of alloy substrate, respectively, and τ_o and l_o are the resistivity and thickness of oxide scale, respectively. Compared with the resistivity of the oxide, the resistivity of the metallic substrate is so small that the contribution of the first term in the above equation can be neglected. The *ASR* of an oxidized metallic interconnect is overwhelmingly dominated by that of the oxide layer on both surfaces so that:

$$ASR=2\tau_o l_o \tag{7}$$

It is clear that the occurrence of cracking, either within the oxide layer or along the scale/substrate interface, and the presence of porosity leads to a significant increase in the ASR of an oxide scale. To facilitate the following derivation, a metallic interconnect is assumed to be free of such flaws so its resistance can be represented by Eq.(7).

The *ASR* of a metallic interconnect is considerably influenced by the growth kinetics of the oxide layer upon its long-term exposure to oxidizing atmospheres. Essentially, the oxidation process involves the chemical reaction of a metal with gaseous oxygen in the atmosphere to yield a layer of protective and thermodynamically stable oxide through either the inward diffusion of oxygen, or the outward diffusion of alloying elements, or both. The thickness of the oxide scale as a function of time (t) at a constant temperature is well documented to obey the general form of (Gonzalez-Carrasco *et al*., 1999; Tortorelli and Natesan, 1998; Montealegre *et al*., 2000; 2001):

$$l_o^n = K_p t \tag{8}$$

where n is an exponent reflecting the oxidation mechanism, and K_p is the growth rate constant that depends upon the absolute temperature (T) and the activation energy for the diffusion (E_{ox}) of rate-limiting species, and can be empirically represented by the following expression:

$$K_p=K_0\exp(-E_{ox}/kT) \tag{9}$$

where K_0 is a pre-exponent constant and k Bolzmann constant. It has established that in most cases, oxide scale growth at steady-stage oxidation follows parabolic law meaning that the exponent n in Eq.(8) equals 2 and K_p is often termed as the parabolic rate constant.

Likewise, the conduction of a metal oxide is a thermally activated process that involves the movement of small polarons via the transport of holes (or vacancies). The electrical resistivity, which is the inverse of conductivity, can be given as:

$$\tau_o = \frac{1}{\sigma} = \frac{T}{\sigma_0 \exp(-E_{co}/kT)} = \frac{T}{\sigma_0}\exp(E_{co}/kT) \quad (10)$$

where σ_0 is a pre-exponent constant, and E_{co} is the activation energy barrier for the conduction process. Therefore, Eq.(7) can be expressed as:

$$ASR = 2\frac{\sqrt[n]{K_p t}}{\sigma_0} T \exp\left(\frac{-E_{ox}/n + E_{co}}{kT}\right) \quad (11)$$

In a situation where the oxide scale thickens in parabolic fashion (Tortorelli and Devan, 1992; Pint, 1996; Devan and Tortorelli, 1993; Pint *et al.*, 1993):

$$ASR = 2\frac{\sqrt{K_p t}}{\sigma_0} T \exp\left(\frac{-E_{ox}/2 + E_{co}}{kT}\right) \quad (12)$$

By plotting ASR/T versus $1/T$ on a logarithmic scale, the activation energy term encompassing the contributions of both oxidation and conduction can be obtained. It can be readily seen that the ASR changes in parabolic manner with time at a fixed temperature. In principle, metals that develop slow-growing oxide scale with high electrical conductivity are highly desired as interconnects. However, for most metal oxides, these two attributes are mutually exclusive (Samsonovin, 1973). Any approach that is designed to suppress the oxidation kinetics and promote the electrical conductivity of the oxide scale in a SOFC-like environment inevitably lowers the ASR value of the interconnect. The approaches that have been demonstrated to be effective in this aspect include: (1) doping the oxide with an oxygen reactive element that alters the overall oxidation mechanism; (2) doping the oxide with heterovalent metal ions that increase the hole concentration; and (3) providing a complex adequately thick oxide coating that is impermeable to oxygen gas.

Prior to examining and comparing the ASRs of various metallic interconnects under current development, and evaluating the prospects of their application to the planar anode-supported SOFC, it is necessary to describe the measurement approach that is well accepted and widely employed in many studies, although some minor details may vary. As shown schematically in Fig.15, basically, the contact resistance of the oxide scale is measured through a two-point, four-wire probe approach. A contact current in the order of ten to several hundred mA is introduced and the voltage across the sample is measured with a multimeter. Different currents are employed initially to establish the fact the system exhibits ohmic behavior. Platinum gauzes are placed onto the test sample using platinum paste and the measurement wires are spot welded to the gauzes. To ensure good contact between the gauze and the surface, an adequate load is applied in the through-thickness direction. In some cases, the platinum paste and gauze are replaced by platinum tab secured through a spring-load of appropriate magnitude.

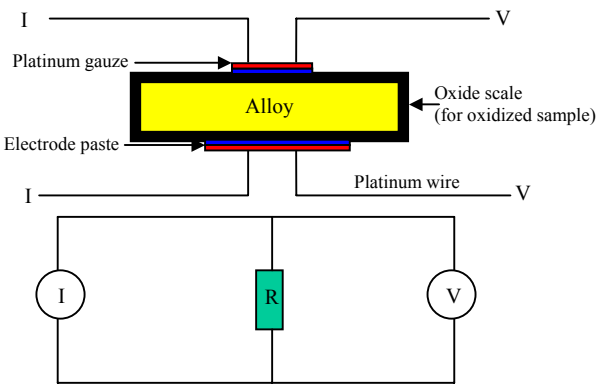

Fig.15 Schematic drawing showing the measurement of contact resistance

Chromium-based alloys

This type of alloy was initially developed for interconnects as the replacement of ceramic interconnects in a planar electrolyte-supported SOFC stack that operates typically around 1000 °C. A representative alloy in this category is Ducrolloy ($Cr\text{-}5Fe\text{-}1Y_2O_3$) that was specifically designed by Plansee Company to match the thermal expansion coefficients of other SOFC components, and at the same time to provide other requisite interconnect characteristics as well (Tiffee *et al*., 1990). More importantly, the reason why the chromia-forming alloys such as Ducrolloy were chosen as potential interconnect candidates is that in relation to other metal oxides, chromia displays relatively high electrical conductivity and reasonably slow growth rate at SOFC operating temperatures. Based on Eq.(7), it is expected that a fairly low ASR could be achieved with this alloy throughout its lifetime service. The alloy is preferably prepared by a powder metallurgy approach to facilitate the mass production at low cost (Glatz *et al*., 1999). As mentioned earlier, the incorporation of oxide into the base composition (also termed oxide dispersed alloys, ODS) was intended to provide improved oxidation resistance, a refined grain size within the scale, an adherent scale/substrate interface, as well as enhanced mechanical properties (Quadakkers *et al*., 1994).

Up to now, considerable studies on the oxidation behavior of Ducrolloy have been performed mainly at temperatures above 900 °C, which is plausible from a standpoint of application. In an oxidizing atmosphere at elevated temperatures, chromia scale develops on the alloy surfaces and effectively acts as a protective layer to alleviate or slow down further Cr dissipation from the substrate. Limited information on the contact resistance of oxidized Ducrolloy (Liebert, 1999) indicates that the ASR of alloy after exposure to air at 1000 °C for 75 h, as shown in Fig.16, is prohibitively large, leading to poor stack performance. It seems that the thickness of the chromia scale formed on the surface of Ducrolloy after oxidation at 1000 °C for 75 h is too large so that the resulting ASR is several orders of magnitude higher than the criterion value. It can be concluded that, without coating, Ducrolloy is unsuitable for application as an interconnect in electrolyte-supported SOFC. The authors are unaware of reports of study on the applicability of Ducrolloy as interconnect for planar anode-supported SOFC whose operating temperature is around 800 °C, because Fe-based or Ni-based chromium-containing alloys are favored over chromium-based ones due to the substantially reduced cost and moderately improved ductility.

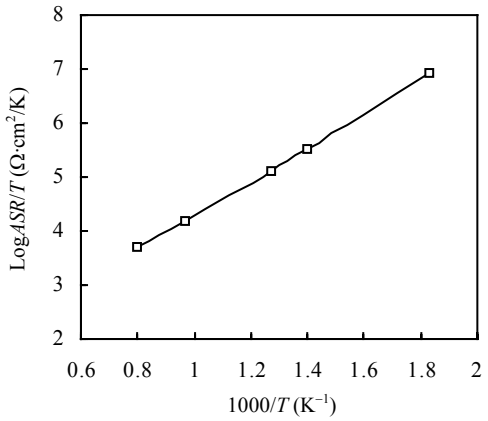

Fig.16 Temperature-dependence of area specific resistance (ASR) of $Cr\text{-}5Fe\text{-}1Y_2O_3$ alloy (Durcrolloy) oxidized at 1000 °C for 75 h in air, showing unacceptably large ASR for practical application as interconnect (Liebert, 1999)

Iron-based alloys

The viability of Fe-based alloys as interconnects also relies on the formation of chromia scale upon their exposure to SOFC operating atmospheres. Another reason for the selection of Fe-based alloys is that their coefficients of thermal expansion can be advantageously matched with those of other SOFC components at an operating temperature of around 800 °C (Hou *et al*., 1999; Brylewski *et al*., 2001; Linderoth *et al*., 1996). The variation of *ASR* as a function of temperature for an Fe-26Cr-1Mo alloy oxidized at 800 °C for 48 h is shown in Fig.17 (Hou *et al*., 1999). The *ASR* value at 800 °C is around 0.015 $\Omega\cdot cm^2$, which is well below the acceptable level. However, as the oxidation time is prolonged to 1000 h, according to Eq.(12) where the parabolic growth behavior of chromia scale is assumed, the *ARS* is predicted to

reach 0.2 $\Omega \cdot cm^2$. This value already exceeded the criterion for practical application, which means that long-term use of this alloy as the interconnect of SOFC at 800 °C operating temperature is unsatisfactory.

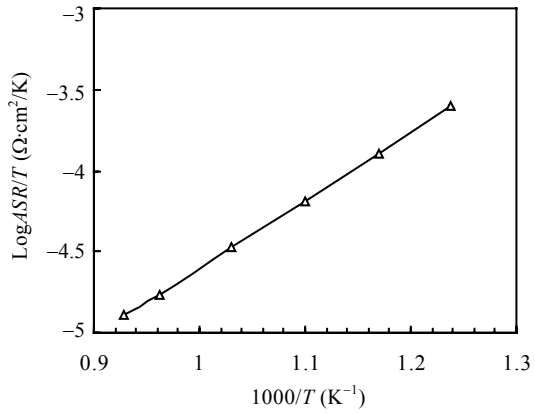

Fig.17 Variation of ASR with temperature for a Fe-26Cr-1Mo alloy oxidized at 800 °C for 48 h in air where Pt electrode was used for measurement (Hou *et al.*, 1999)

It should be stressed that the electrical conductivity of Cr_2O_3 formed on Fe-based alloys is usually lower than what would be expected for a Cr_2O_3 crystal that formed on Cr-based alloys. This is explained by the fact that the electrical conductivity of the chromia scale is dominated by impurities, in this case Fe, and essentially exhibits extrinsic behavior while that of pure chromia is intrinsic in nature.

The compatibility between alumina-forming FeCrAl alloys and $La_{1-x}Sr_xMnO_3$ which is a well-established and widely accepted cathode material for SOFC, had been examined (Quadakkers *et al.*, 1996). It was revealed that a duplex interface layer consisting of alumina and a mixed oxide of Al, La, and Mn is formed after the layer's exposure to air at elevated temperature. The electrical resistance of the metal/ceramic couple increases by a factor of 100 after 1000 h exposure at 900 °C, which suggests that FeCrAl-based alloys are also highly unsuitable for interconnects at this temperature due to the development of an insulating alumina scale. Further study on the development of the oxide scale and its contact resistance at 800 °C should be carried out.

The electrode materials used for the conductivity measurement exert a pronounced effect on the final results, as illustrated in Fig.18 for an Fe-26Cr-1Mo alloy (Huang *et al.*, 2000). This is especially true when one monitors the variation of *ASR* with time continuously at an oxidation temperature. With a Pt electrode, the scale shows the lowest *ASR*, and this increases nearly parabolically with time. With a mixed *LSM* ($La_{0.85}Sr_{0.15}MnO_3$)+ *LSGM* ($La_{0.80}Sr_{0.20}Ga_{0.83}Mg_{0.17}O_{2.85}$) electrode, the scale displays an intermediate *ASR* value that moderately deviates from parabolic behavior. With LSCo ($La_{0.6}Sr_{0.4}CoO_3$), the *ASR* value was the largest, and deviates significantly from a parabolic dependence. The large *ASR* resulting from using ceramic electrodes is mainly ascribed to the reaction of the electrodes with the alloy to form porous spinel phase during measurement. This concern can be address by depositing the ceramic electrodes onto pre-oxidized alloy so that the chromia scale can effectively separate the electrode from the alloy surface. However, the Pt electrode is still preferred over ceramic electrodes because the relatively high resistance of the ceramic electrode itself, along with a larger interfacial resistance due to poor bonding between the electrode and oxide scale, can contribute to a large measured *ASR*, as can be seen from Fig.18. Fig.19 further highlights the impact of different electrodes on the measured *ASR* (Huang *et al.*, 2000). Despite the difference in measured values, the linear dependence of log(*ASR*/*T*) on 1/*T* is still roughly maintained.

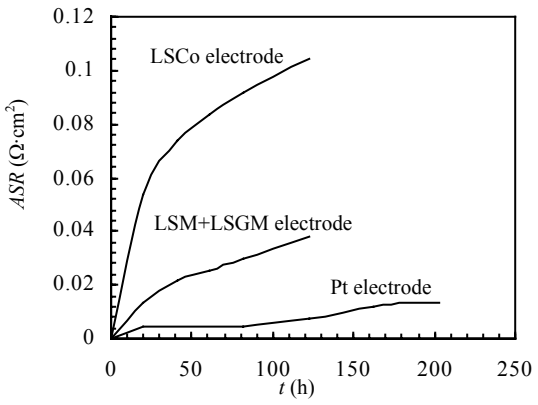

Fig.18 Variation of ASR with time measured at 850 °C in air with three different electrodes on the surfaces of unoxidized Fe-26Cr-1Mo alloy (Huang *et al.*, 2000)

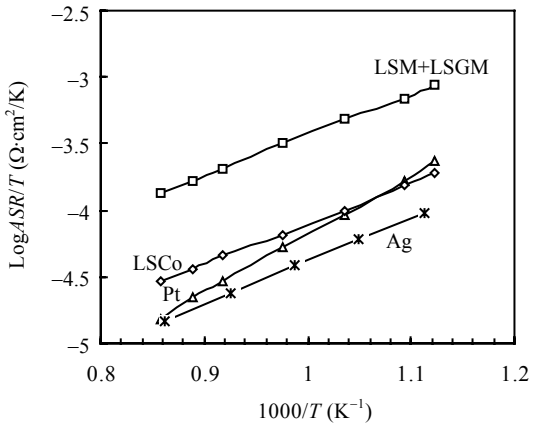

Fig.19 Dependence of ASR on temperature for a Fe-26Cr-1Mo alloy pre-oxidized at 900 °C for 24 h measured with four different electrodes (Huang *et al.*, 2000)

Doping with such elements as Y, Zr, La, Hf and Ce can effectively reduce the *ASR* of the oxide scale. The criterion for selecting the doping elements depends on the type of oxide scale formed on the oxidized alloy surface. The experimental results (Hou *et al.*, 1999) for a Fe-26Cr-1Mo alloy, as shown in Fig.20, indicate that Y-doping decreases the *ASR*. This is due to the reduced growth rate of chromia, as well as a more adherent scale/substrate interface. The pronounced reduction in *ASR* associated with Ni-doping is due to the increased hole concentration in the scale, which serves as additional evidence that the conductivity of chromia is extrinsic.

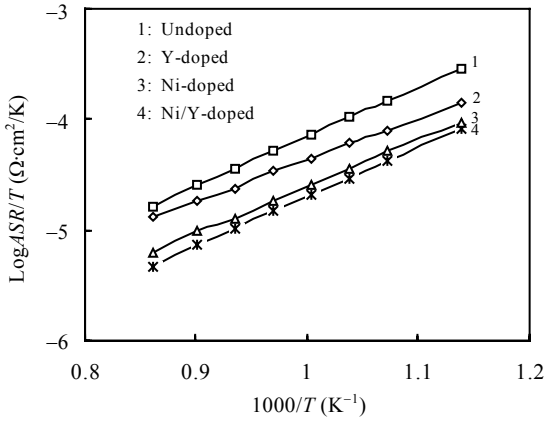

Fig.20 Temperature-dependence of area specific resistance for undoped and doped Fe-26Cr-1Mo alloy oxidizd at 800 °C for 24 h in air where Pt electrode was used for measurement

Co-doping with Y and Ni combines the beneficial effect of Ni on conductivity with that of Y on oxidation, thus leading to further decrease in *ASR*. Consequently, it is suggested that Ni-based Cr-bearing alloys are favored as interconnects from an *ASR* point of view, although Fe-based alloys usually have more compatible thermal expansion coefficients compared with those of other ceramic cell components.

Nickel-based superalloys

Applicability of some commercially available Ni-based superalloys as interconnects was assessed in both oxidizing and reducing atmospheres (Linderoth *et al.*, 1996; Vazquez-Navarro *et al.*, 1999). Virkar and Kim (2001) examined the oxidation kinetics of thin foils and the ASRs of the oxide scales formed on the surfaces. The justification for the use of thin foil metallic interconnects is that thin foil Ni-based alloys are compliant and flexible enough to withstand the thermal stresses arising from the mismatch of coefficients of thermal expansion among cell components. All the compositions studied obey a parabolic rate law of oxidation at 800 °C, indicating a diffusion-controlled process. Haynes 230 exhibits the slowest oxidation kinetics, forming an oxide scale that consists predominantly of a major Cr_2O_3 phase, and a minor spinel phase ($Mn_{1+\delta}Cr_{2-\delta}O_{4-\lambda}$) (England and Virkar, 1999). It is, therefore, not surprising that oxidized Haynes 230 displays the lowest *ASR* at 800 °C, as shown in Fig.21 (England and Virkar, 1999). It is further inferred that the existence of a complex oxide in the form of Cr_2MnO_4 is advantageous in reducing the ASR of the scale. Their experiments demonstrated that the oxidation occurs not only in the cathodic atmosphere, but also in the fuel atmosphere. This is because the typical partial pressure of oxygen in the fuel used in an SOFC ranges from 10^{-22} to 10^{-17} atm, depending on the temperature and fuel composition. By contrast, the equilibrium partial pressure of oxygen for Cr/Cr_2O_3 is several orders of magnitude lower (10^{-28} atm at 800 °C), i.e., Cr_2O_3 is thermodynamically more stable than the Cr present in the alloy so that formation of Cr_2O_3 is favored. The *ASR* of an oxide scale formed in a typical fuel

atmosphere is lager than that of an oxide scale formed in air under identical temperature and time, which may be seen from comparison of Fig.22 with Fig.23 (England and Virkar, 1999; 2001). The underlying reason for this phenomenon still remains to be clearly identified. It is speculated that due to the presence of water, the oxide scale formed in the humid fuel is prone to be porous and poorly adhered to the substrate. Besides, chromia scale might have larger electrical resistivity in reducing atmosphere as compared to oxidizing atmosphere.

An Mn-based coating on the anode-facing side of metallic interconnects made from superalloys like Haynes 230 was conceived to suppress the for mation of chromia and reduce the ASR of the scale and experimentally tested (Virkar and England, 2000). As demonstrated in Fig.24, after being exposed to wet hydrogen at 800 °C for 100 h, the Mn-coated Haynes 230 exhibits a significantly lowered *ASR* compared to the uncoated sample. This is attributable to the formation of $MnCr_2O_4$ that has a much lower electrical resistivity. The presence of an oxide comprising predominantly $MnCr_2O_4$ is highly favorable for the operation of metallic interconnects in both reducing and oxidizing gases. However, it is yet to be determined whether coatings like this can still remain adhered to the substrate to withstand thermal cycling that is likely to be frequently encountered in practical SOFC operation. Another issue that needs to be

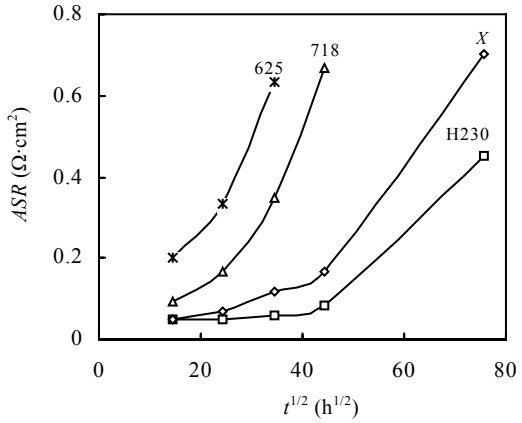

Fig.21 Area-specific resistance vs (oxidation time)$^{1/2}$ for various Ni-based superalloys oxidized at 800 °C (England and Virkar, 1999)

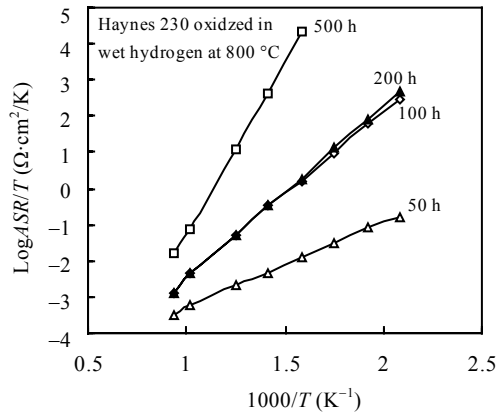

Fig.22 Area specific resistance of Haynes 230 oxidized at 800 °C in wet hydrogen for various periods of time as a function of measuring temperature(from 200 °C to 800 °C) (England and Virkar, 1999)

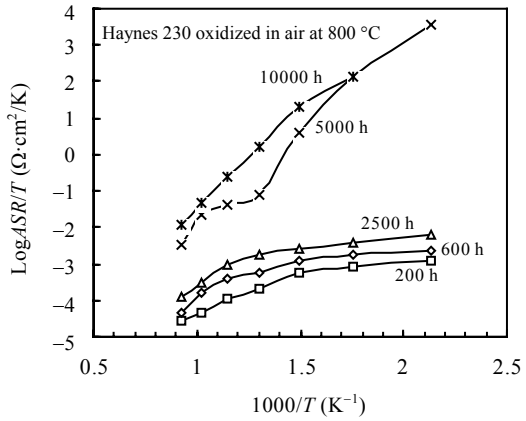

Fig.23 Area specific resistance of Haynes 230 oxidized at 800 °C in air for various peroids of time as a function of measuing temperature (from 200 °C to 800 °C) (England and Virkar, 2001)

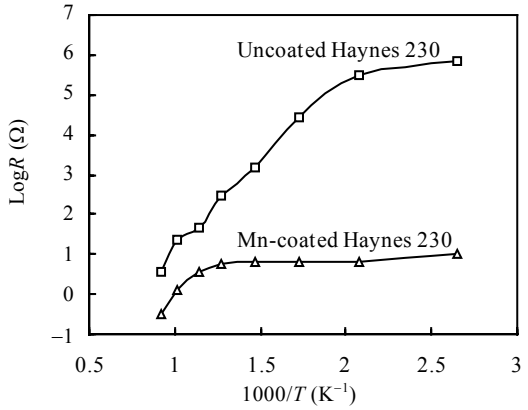

Fig.24 Temperature-dependence of electrical resistance of Haynes 230 and Mn-coated Haynes 230 after exposure to wet hydrogen at 800 °C for 100 h (Virkar and England, 2000)

addressed is the long time growth kinetics of the complex oxides, preferably corresponding to the service time of the SOFC, which is vital to their ultimate usefulness. It can be seen from Fig.23 that the *ASR* of 1.1 Ω·cm^2 at 800 °C for 10000 h of oxidation of Haynes 230 in air is still unsatisfactory for an SOFC where a stable performance over the expected lifetime (4 years) is required.

The effect of doping with reactive elements like La and Hf on the oxidation mechanism and the *ASR* of the scale was also investigated in chromia-forming Inconel 600 (Oishi and Yamazaki, 1999). It was revealed that in the presence of La, the Cr in the alloy is oxidized internally, rather than externally. In both fuel and air atmospheres, the *ASR* can be lowered by one order of magnitude by La doping, as shown in Fig.25. It is suggested that the electrical conduction mechanism of chromia might have been modified by La-doping, which is supported by the observation that the activation energy for the electrical conduction of the doped sample is lower than that of undoped one in both atmospheres.

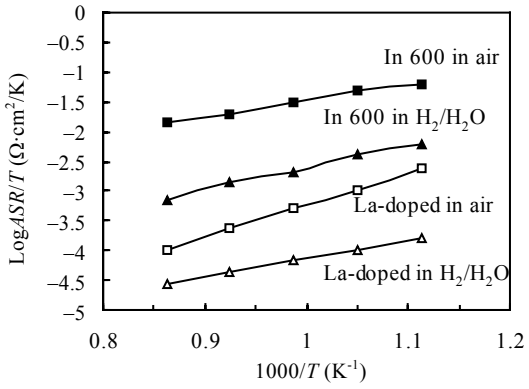

Fig.25 Temperature-dependence of *ASR* of oxide scale grown on the undoped and La-doped In 600 after oxidation at 900 °C in different atmospheres for 200 h (Oishi and Yamazaki, 1999)

The most severe problems encountered with Ni-based Cr-containing alloys, and in general, all chromia-forming alloys proposed as interconnect candidates are considered: (1) unacceptably high oxidation rate; (2) occurrence of buckling and spallation of the oxide scale when subjected to thermal cycling; and (3) volatization of high valence Cr-species in the form of CrO_3, or $Cr(OH)_2O_2$. The first two will detrimentally result in a significant increase in the *ASR*. The last one will poison the air electrode because of the reduction of volatile Cr (VI) species to solid Cr (III) oxide at the cathode/electrolyte interface, as well as along the pores, and lead to rapid deterioration of cell performance due to the substantial increase in both concentration and activation polarizations (Badwal *et al*., 1997; Matsuzaki and Yasuda, 2000). Additionally, special precautions must be taken during the startup of the SOFC stack in which chromia-forming interconnects are utilized in combination with Ni anodes. NiO reacts much more readily with Cr_2O_3 than perovskite chromite to form Ni-Cr spinels. Although the spinel is reduced during anode reduction, the formation seems to result in the appearance of large Cr_2O_3 crystals. This could cause alignment problems between adjacent surfaces in the stack during operation, and hence increase contact resistance.

Effect of coating

In order to reduce the rate of scale growth on the surfaces of chromia-forming alloys, as well as prevent the chromium vaporization on the cathode side, coating with a perovskite or spinel ceramic layer by thermal spraying has been suggested and currently is being extensively investigated (Brylewski *et al*., 2001; Quadakkers *et al*., 1996; Batawi *et al*., 1999a; 1999b; Honegger *et al*., 2002; Yoo and Daugo, 2002; Janousek *et al*., 1997). Another option is to coat these alloys with an oxide layer that subsequently reacts with chromia to form a chromite (or chromate). The resulting compound should exhibit better electrical conductivity as compared to chromia and be capable of retarding further oxidation of chromium and suppressing the volatilization of chromium. Since this in-situ approach suffers the obvious drawback of difficulty in controlling the composition of the reaction product, coating with perovskite or spinel oxides directly on the surfaces of the metallic interconnects is preferred. To qualify as a viable coating material, it should possess the following attributes: (1) The diffusion coefficients of Cr and O in the coating

should be as small as possible so that the transport of chromium and oxygen can be effectively hindered. The spinel oxide might be a better choice than the perovskite one because the former is more effective in preventing the oxygen diffusion; (2) It should be chemically compatible and stable with respect to substrate and electrodes; (3) It should be thermodynamically stable in both oxidizing and reducing atmospheres over the applied temperature range; (4) It must have low ohmic resistance to maximize electrical efficiency; (5) The thermal expansion coefficient should be well matched to the substrate so that the coating is resistant to spallation during thermal cycling. Currently, Sr-doped $LaCrO_3$ (LSC) and $LaMnO_3$ (LSM) are the most favored coating materials, although cheaper substitutes are being sought for.

Presented in Fig.26 is the dependence of contact resistance with respect to time at 920 °C for various Cr-based ODS alloys coated with LSM (Batawi *et al*., 1999b). The presence of an LSM coating is crucial in maintaining the low level of contact resistance at elevated temperatures over extended periods of time. Equally low contact resistance was also reported (Honegger *et al*., 2002) on LSM coated Fe-based superalloys at 800 °C for even longer periods of time, as shown in Fig.27. Compatibility between the LSM coating layer and the Cr-5Fe-1Y_2O_3 alloy was also investigated at elevated temperatures for prolonged times (Quadakkers *et al*., 1996). Reaction between the interconnect alloy and the coating to form spinel may occur via solid-state diffusion, as well as volatile of transport oxides and/or hydroxides. This phenomenon can be tolerated as long as the time for the diffusion of chromium through the coating is longer than the required service lifetime. Results by Quadakkers *et al*.(1996) as shown in Fig.28 indicates that an LSM coating on MA-956 (an FeCrAlY) can reduce the contact resistance by roughly three orders of magnitude, implying that the LSM coating is very effective in slowing down the oxidation kinetics of the metallic species in the alloy. In addition to LSM, coating materials such as LSC, Sr-doped lanthanum cobalt (LSCo), and Sr-doped lanthanum iron cobalt (LSFeCo) have been established to be highly advantageous in decreasing the ASR, as shown in Fig.29 (Yoo and Daugo, 2002).

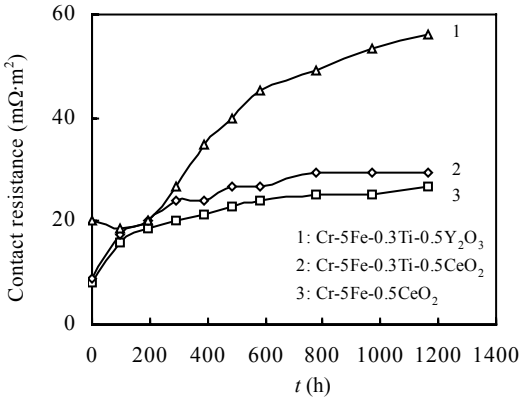

Fig.26 Changes of contact resistance as a function of time at 920 °C for various Cr-based ODS alloys coated with LSM (Batawi *et al.*, 1996b)

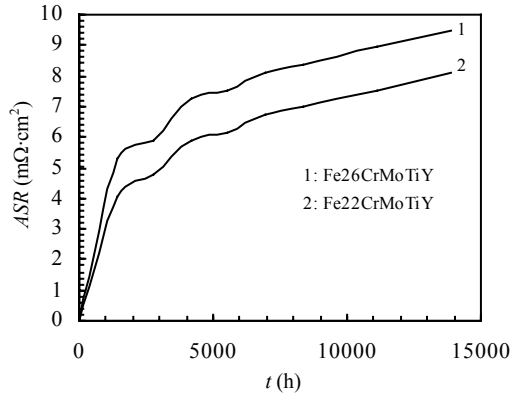

Fig.27 Variation of ASR of two LSM coated Fe-based superalloys with time at 800 °C (Quadakkers *et al.*, 1996)

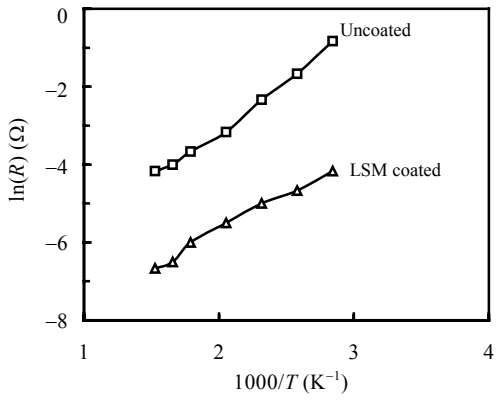

Fig.28 Temperature-dependence of contact resistance of both uncoated and LSM-coated MA-956 alloy after 1000 h exposure to air at 900 °C (Quadakkers *et al.*, 1996)

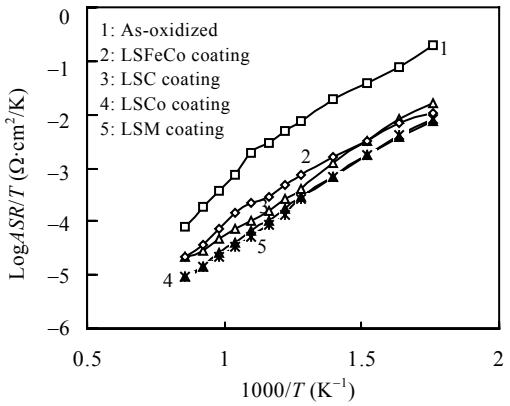

Fig.29 Effect of different coatings on ASR of the Fe-28Cr-3Mo alloy after oxidation at 950 °C for 10 h as a function of temperature (Yoo and Daugo, 2002)

PROCESSING OF METALLIC INTERCONNECTS

Metallic interconnects are always utilized in the form of sheet in flat SOFC design. Although the use of thin foil Ni-based superalloys has been proposed and tested, the choice of 4–5 mm thick sheet is favored from the machining standpoint since both fuel and oxidant channels can be integrated into the sheet. Preparation of metallic interconnects with desired properties using inexpensive processing approaches is one of the critical factors determining the successful commercialization of SOFC technique. For Fe- and Ni-based superalloys, the well-developed melt metallurgy techniques for industrial mass production can be applied to manufacture preformed semifinished interconnect. The preformed part is subsequently subject to mechanical machining or advanced shaping technique such as electrochemical machining (ECM) to become the finished part. In this circumstance, the machining cost accounts for a significant portion of the overall cost of the interconnect. When it comes to the Cr-based alloys, due to the inherent hindrances associated with the Cr-melt metallurgy such as high melting point, high reactivity, and high evaporation rate of molten chromium, powder metallurgy (PM) processing is a preferred route for sheet manufacture. PM-manufacture offers the advantage of easy amplification for industrial scale production. It offers additional flexibility in alloy and interconnect design. With specific reference to the oxide-dispersed Cr-based alloys, the distribution of dispersoid like Y_2O_3 that is purposely incorporated to confer desired oxidation properties can be remarkably improved by PM-processing.

Traditional PM processing involves hot rolling the pressed and sintered powder precompacts to sheet materials followed by the gas channel construction and surface polishing using mechanical machining or ECM (Janousek *et al*., 1997). This route is particularly suitable for preparing large area sheet with thickness ranging from 1.5 mm to 10 mm. Alternately, the consolidation of near-net-shaped powder preform is accomplished by hot isostatic pressing (HIP) followed by multi-wire sawing of plate-shaped material. The finalized components with grooves for gas transport are made available by using mechanical machining or ECM technique. Since the multi-wire sawing technique is time consuming and costly especially with regard to large-scale preform, this route is limited to manufacturing sheet with diameter of less than 300 mm. In either case, the mixture of powder raw materials (chromium, iron and yttria in the instance of Durolloy) is achieved by either simple mixing or mechanical alloying in a high-energy ball mill. Mechanical alloying provides the attendant benefit of reducing the particle size and improving the distribution of oxides.

A net-shape PM processing technique has been recently developed in an attempt to reduce the cost associated with post-sintering/post-rolling ECM in the classical PM (Glatz *et al*., 1999; 2000; 2001). This approach essentially consists of net-shape pressing of prealloyed raw materials and subsequent sintering and brazing of the precompacted pellets. Depending on the quality of the sintered interconnects, mechanical machining sometimes is needed to obtain the required precision. To curtail or eliminate dependence on ECM for gas channel buildup in the finished components, the requirement for the powder characteristics to achieve a maximum density of the finished interconnect along with a homogenous density distribution is exceptionally stringent, particularly when the flat

components with complex gas channel configuration are considered. A number of factors are identified to determine the achievable sintering density and should be optimized via repeated tests. These in due include but are not limited to purity of raw materials, powder morphology, average particle size and size distribution, alloy composition, pressing parameters, and sintering parameters. The net-shape PM technique is proved to be competitive in manufacturing small or medium-sized metallic interconnects. The significantly reduced final machining characteristic of this approach leads to considerable material saving and a drastic drop of the machining cost. A projected cost reduction potential of at least an order of magnitude in the industrial scale production as compared to conventional PM technique has been demonstrated. The performance of a 5-cell stack equipped with metallic interconnects made of Durolloy manufactured by net-shape PM was evaluated up to 1000 h as shown in Fig.30 (Glatz *et al*., 1999). Prior to being installed, the interconnects were coated with a protective LSM layer using thermal spray. It is encouraging to note that stack with net-shape PM interconnect displays identical electrochemical performance stability to the one fitted with conventional PM interconnects. No discernible performance degradation was observed during the entire test.

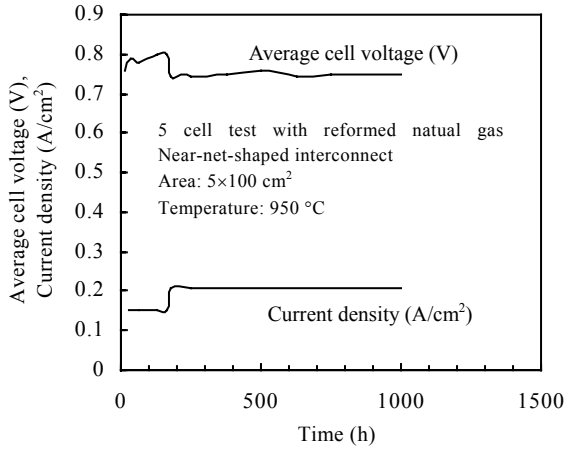

Fig.30 Performance of a 5-cell SOFC stack equipped with an interconnect fabricated using near-net-shaped powder metallurgy technique, the interconnect is made from Cr-5Fe-1Y_2O_3 alloy (Glatz *et al*., 1999)

One proposed technique to fabricate thin foil Cr- or Fe/Cr-based metallic interconnects is tape-casting (Glatz *et al*., 2000). Tape-casting is a well-established, low-cost manufacturing approach widely utilized in the electronic ceramic industry to manufacture multi-layer ceramic capacitors. The SOFC electrolyte is presently being fabricated exclusively by using this technique. The selection of appropriate dispersants and binders and optimization of their amounts added for specific material are of paramount importance in achieving a stable slurry with desired casting properties. Green tapes with thickness in the range of 0.4–1 mm are consolidated by sintering. Depending on the sintered density of the sheet material, a post-sintering compaction treatment by rolling is recommended in order to achieve further densification and thickness reduction. Results indicated that some specifically adapted Cr-based alloy powders show tape-casting behavior comparable to that of ceramic powders.

CONCLUDING REMARKS

Successful development of interconnect materials is vital to the large-scale commercialization of SOFCs technology. The growing trend toward the anode-supported planar version in the SOFC community shows great promise for the use of metallic interconnects. To address the challenge of excessively large contact resistance on short exposure to SOFC environments, new metallic interconnects should be developed based on a fundamental understanding of oxide growth kinetics and oxide conductivity. This should be the focus of future study. Other recommended avenues of investigation include further lowering the operating temperature of SOFC to 700 °C or even 600 °C without compromising the fuel cell electrical efficiency. This essentially allows current commercially available stainless steels to be utilized directly as interconnects. Coating metallic interconnects with oxides of complex structure has proved to an effective approach to reduce the contact resistance. This practice can be put into widespread application provided that costs of both coating

materials and fabrication techniques are substantially curbed.

References

Anderson, H.U., Murphy, R., Humphrey, K., Rossing, B., Aldred, A., Procarioue, W.L., Ackermann, R.J., 1978. *In*: McCarthy, G.J., Rhyne, J.J. (Eds.), The Rare Earths in Modern Science and Technology. Plenum Press, New York, p.55.

Anderson, H.U., Nasrallah, M.M., Flandermeyer, B.K., Agarwal, A.K., 1985. *J. Sol. Stat. Chem.*, **56**:325.

Anderson, H.U., Kuo, J.H., Sparlin, D.M., 1989. *In*: Proceedings of the First International Symposium on Solid Oxide Fuel Cells, PV89-11, The Electrochemical Society Proceedings Series. Pennington, NJ, p.111.

Armstrong, T.R., Stevenson, J.W., Pederson, L.R., Raney, P.E., 1995. *In*: Proceedings of the Fourth International Symposium on Solid Oxide Fuel Cells (SOFC-IV). The Electrochemical Society Proceedings Series. Pennington, NJ, p.944.

Armstrong, T.R., Stevenson, J.W., Pederson, L.R., Raney, P.E., 1996a. *J. Electrochem. Soc.*, **143**:2919.

Armstrong, T.R., Stevenson, J.W., Pederson, L.R., 1996b. *In*: Proceedings of Second European Solid Oxide Fuel Cell Forum. Oslo, Norway, **2**:521.

Armstrong, T.R., Hardy, J.S., Simner, S.P., Stevenson, J.W., 1999. *In*: Proceedings of the Sixth International Symposium on Solid Oxide Fuel Cells (SOFC-VI). Honolulu, Hawaii, p.706.

Badwal, S.P.S., 2001. *Sol. Stat. Ion.*, **143**:39.

Badwal, S.P.S., Deller, R., Foger, K., Ramprakash, Y., Zhang, J.P., 1997. *Sol. Stat. Ion.*, **99**:297.

Barthel, K., Rambert, S., Siegmann, S., 2000. *J. Therm. Spray Technol.*, **9**:343.

Batawi, E., Honegger, K., Diethelm, R., Wettstein, M., 1996. *In*: Proceedings of Second European Solid Oxide Fuel Cell Forum. Oslo, Norway, **2**:307.

Batawi, E., Plas, A., Straub, W., Honegger, K., Diethelm, R., 1999a. *In*: Proceedings of the Sixth International Symposium on Solid Oxide Fuel Cells (SOFC-VI). Honolulu, Hawaii, p.767.

Batawi, E., Glatz, W., Kraussler, W., Janousek, M., 1999b. *In*: Proceedings of the Sixth International Symposium on Solid Oxide Fuel Cells (SOFC-VI). Honolulu, Hawaii, p.731.

Bates, J.L., 1990. *In*: Proceedings of the Second Annual Fuel Cells Contractors Review Meeting. Rept. No. DOE/METC-90/6112, U.S. Department of Energy, Washington DC, p.159.

Boroomand, F., Wessel, E., Singheiser, L., Hilpert, K., 1999. *In*: Proceedings of the Sixth International Symposium on Solid Oxide Fuel Cells (SOFC-VI). Honolulu, Hawaii, p.666.

Bredesen, R., Kofstad, P., 1996. *In*: Proceedings of Second European Solid Oxide Fuel Cell Forum. Oslo, Nroway, **2**:567.

Brylewski, T., Nanko, M., Maruyama, T., Przybylski, K., 2001. *Sol. Stat. Ion.*, **143**:131.

Chen, H.C., Heberlein, J., Hene, R., 2000. *J. Therm. Spray Technol.*, **9**:348.

Chick, L.A., Bates, J.L., Pederson, L.R., Kissinger, H.E., 1989. *In*: Proceedings of the First International Symposium on Solid Oxide Fuel Cells. The Electrochemical Society, Pennington, NJ, p.170.

deHaart, L.G.L., Vinke, I.C., Janke, A., Ringel, H., Tietz, F., 2001. *In*: Proceedings of the Seventh International Symposium on Solid Oxide Fuel Cells (SOFC-VII). Tsukuba, Ibaraki, Japan, p.111.

Devan, J.H., Tortorelli, P.F., 1993. *Corros. Sci.*, **35**:1065.

Dollard, W.J., Brown, J.T., 1986. Overview of the Westinghouse Solid Oxide Fuel Cell Program, Fuel Cell Abstracts. Fuel Cell Seminar. Tucson, AZ,

Dulieu, D., Cotton, J., Greiner, H., 1998. *In*: Proceedings of Third European Solid Oxide Fuel Cell Forum. Nantes, France, p.447.

Elangovan, S., Hartvigsen, J.J., Kung, S.C., Goettler, R.W., Barringer, E.A., 2001. *In*: Proceedings of the Seventh International Symposium on Solid Oxide Fuel Cells (SOFC-VII). Tsukuba, Japan, p.94.

England, D.M., Virkar, A.V., 1999. *J. Electrochem. Soc.*, **146**:3196.

England, D.M., Virkar, A.V., 2001. *J. Electrochem. Soc.*, **148**:A330.

Flandermeyer, B.K., Nasrallah, M.M., Agarwal, A.K., Anderson, H.U., 1984. *J. Am. Ceram. Soc.*, **67**:195.

Flandermeyer, B.F., Nasrallah, M.M., Sparlin, D.M., Anderson, H.U., 1985a. *High Temp. Sci.*, **20**:259.

Flandermeyer, B.F., Nasralk, M.M., Sparlin, D.M., Anderson, H.U., 1985b. *In*: Simkovich, G., Stubican, V.S. (Eds.), Transport Nonstoichiometric Compounds. Plenum Press, New York, p.17.

Foger, K., Donelson, R., Ratnaraj, R., 1999. *In*: Proceedings of the Sixth International Symposium on Solid Oxide Fuel Cells (SOFC-VI). Honolulu, Hawaii, p.95.

Glatz, W., Batawi, E., Janousek, M., Kraussler, W., Zach, R., Zobl, G., 1999. *In*: Proceedings of the Sixth International Symposium on Solid Oxide Fuel Cells (SOFC-VI). Honolulu, Hawaii, p.783.

Glatz, W., Janousek, M., Batawi, E., Honegger, K., 2000. *In*: Proceedings of Fourth European Solid Oxide Fuel Cell Forum. Lucerne, Switzerland, **2**:482.

Glatz, W., Janousek, M., Batawi, E., Doggwiler, B., 2001. *In*: 15th International Plansee Seminar. Reutte, Austria, p.1.

Godfrey, B., Gillespie, R., Foger, K., 1999. *In*: Proceedings of the Sixth International Symposium on Solid Oxide Fuel Cells (SOFC-VI). Honolulu, Hawaii, p.75.

Gonzalez-Carrasco, J.L., Perez, P., Adeva, P., Chao, J., 1999. *Intermetallics*, **7**:69.

Hendriksen, P.V., Carter, J.D., Mogensen, M., 1995. *In*: Proceedings of the Fourth International Symposium on Solid Oxide Fuel Cells (SOFC-IV). The Electrochemical Society Proceedings Series. Pennington, NJ, p.934.

Hiei, Y., Yamamoto, T., Itoh, H., Watanabe, T., 1999. *In*: Proceedings of the Sixth International Symposium on Solid Oxide Fuel Cells (SOFC-VI). Honolulu, Hawaii, p.716.

Hilpert, K., Das, D., Miller, M., Peck, D.H., Weib, R., 1996. *J. Electrochem. Soc.*, **143**:3642.

Hirschenhofer, J.H., Stauffer, D.B., Engleman, R.R., Klett, M.G. (Eds.), 1998. Fuel Cell Handbook. U.S. Department of Energy, Morgantown, WV, p.1-3.

Hofer, H.E., Kock, W.F., 1993. *J. Electrochem. Soc.*, **140**:2889.

Honegger, K., Plas, A., Diethelm, R., Glatz, W., 2002. *In*: Proceedings of the Seventh International Symposium on Solid Oxide Fuel Cells (SOFC-VII). Tsukuba, Ibaraki, Japan, p.803.

Hou, P.Y., Huang, K., Bakker, W.T., 1999. *In*: Proceedings of the Sixth International Symposium on Solid Oxide Fuel Cells (SOFC-VI). Honolulu, Hawaii, p.737.

Hsu, M., 1978. *In*: Proceedings of the Workshop on High-Temperature Solid Oxide Fuel Cells. Rep. No. BNL50756. Brookhaven National Laboratory, Upton, NY, p.127.

Hsu, M., 1985. Fuel Cell Seminar Abstracts (Tucson, AZ, May19-22, 1985). Courtesy Associates, Washington, DC, p.57.

Huang, K.Q., Hou, P.Y., Goodenough, J.B., 2000. *Sol. Stat. Ion.*, **129**:237.

Janousek, M., Kock, W., Baumgartner, M., Greiner, H., 1997. *In*: Proceedings of the Fifth International Symposium on Solid Oxide Fuel Cells (SOFC-V). Aachen, Germany, p.1225.

Kabs, H., Stimming, U., Stovers, D., 1997. *In*: Proceedings of the Fifth International Symposium on Solid Oxide Fuel Cells (SOFC-V). Aachen, Germany, p.160.

Karim, D.P., Aldred, A.T., 1979. *Phys. Rev.*, **B20**:2255.

Khandkar, A., Elangovan, S., 1991. *In*: Proceedings of the Second Annual Fuel Cells Contractors Review Meeting. U.S. DOE/METC, p.152.

Khandkar, A., Elvangovan, S., Hartvigsen, J., Rowley, D., Privette, R., 1999. *In*: Proceedings of the Sixth International Symposium on Solid Oxide Fuel Cells (SOFC-VI). Honolulu, Hawaii, p.88.

Kim, J.W., Virkar, A.V., Fung, K.Z., Mehta, K., Singhal, S.C., 1999. *J. Electrochem. Soc.*, **146**:69.

Flandermeyer, B.K., Dusek, J.T., Blackburn, P.E., Dees, D.W., McPheeters, C.C., Poeppel, R.B., 1986. Fuel Cell Seminar Abstracts (Tucson, AZ, Oct.26-29, 1986). Courtesy Associates, Washington, DC, p.68.

Kofstad, P., 1996. *In*: Proceedings of Second European Solid Oxide Fuel Cell Forum. Oslo, Norway, **2**:479.

Kononyuk, I.F., Tolochko, S.P., Surmach, N.G., 1986. *Neorg. Mater.*, **22**:98.

Krogh, B., Brustad, B., Dahle, M., Eilertsen, J.L., Odegard, R., 1997. *In*: Proceedings of the Fifth International Symposium on Solid Oxide Fuel Cells (SOFC-V). Aachen, Germany, p.1234.

Kuroishi, M., Furuya, S., Hiwatashi, K., 2001. *In*: Proceedings of the Seventh International Symposium on Solid Oxide Fuel Cells (SOFC-VII). Tsukuba, Japan, p.88.

Liebert, B.E., 1999. *In*: Proceedings of the Sixth International Symposium on Solid Oxide Fuel Cells (SOFC-VI). Honolulu, Hawaii, p.722.

Lindermann, G., Boeder, H., Geier, H., 1995. *Adv. Sci. Technol.*, **3D**:2605.

Linderoth, S., Hendrksen, P.V., Mogensen, M., Langvad, N., 1996. *J. Mater. Sci.*, **31**:5077.

Lunghi, P., Ubertini, S., 2001. *In*: Proceedings of the Seventh International Symposium on Solid Oxide Fuel Cells (SOFC-VII). Tsukuba, Ibaraki, Japan, p.254.

Maskalick, N., 1992. Contaminant Effects in Solid Oxide Fuel Cells. Proceedings of the Fourth Annual Fuel Cells Contractors Review Meeting. U.S. DOE/METC.

Matsuzaki, Y., Yasuda, I., 2000. *Sol. Stat. Ion.*, **132**:271.

Meadowcroft, D.B., 1969. *Br. J. Appl. Phys.*, **2**:1225.

Meadowcroft, D.B., 1973. *In*: International Conference on Strontium Containing Compounds. Atlantic Research Institute, Halifax, Canada, p.119.

Meschke, F., Singheiser, L., Steinbrech, P.W., 2000. *In*: Proceedings of Fourth European Solid Oxide Fuel Cell Forum. Lucerne, Switzerland, **2**:865.

Minh, N.Q., 1993. *J. Am. Ceram. Soc.*, **76**:563.

Minh, N.Q., Takahashi, T., 1995. Science and Technology of Ceramic Fuel Cells. Elsevier, Amsterdam.

Minh, N.Q., Horne, C.R., Liu, F.S., Moffatt, D.M., Staszak, P.R., Stillwagon, T.L., VanAckeren, J.J., 1990. *In*: Proceedings of the Twenty Fifth Intersociety Energy Conversion Engineering Conference. American Institute of Chemical Engineers, New York, **13**:256.

Mizusaki, J., Yamauchi, S., Fueki, K., Ishikawa, A., 1984. *Sol. Stat. Ion.*, **12**:119.

Montealegre, M.A., Gonzalez-Carrasco, J.L., Munoz-Morris, M.A., Chao, J., 2000. *Intermetallics*, **8**:439.

Montealegre, M.A., Gonzalez-Carrasco, J.L., Munoz-Morris, M.A., 2001. *Intermetallics*, **9**:487.

Mori, M., Hiei, Y., Sammes, N.M., 1999. *Sol. Stat. Ion.*, **123**:103.

Mori, K., Miyamoto, H., Takenobu, K., Matsudain, T., 2000. *In*: Proceedings of Fourth European Solid Oxide Fuel Cell Forum. Lucerne, Switzerland, **2**:875.

Mukerjee, S., Grieve, M.J., Haltiner, K., Faville, M., 2001.

In: Proceedings of the Seventh International Symposium on Solid Oxide Fuel Cells (SOFC-VII). Tsukuba, Ibaraki, Japan, p.173.

Natesan, K., 1998. *Mater. Sci. Eng.*, **A258**:126.

Nernst, W., 1899. *Z. Elektrochem*, **6**:41.

Oishi, N., Yamazaki, Y., 1999. *In*: Proceedings of the Sixth International Symposium on Solid Oxide Fuel Cells (SOFC-VI). Honolulu, Hawaii, p.759.

Okumura, K., Ailhara, Y., Ito, S., Kawasaki, S., 2000. *J. Therm. Spray Technol.*, **9**:354.

Park, J.W., Lee, Y.K., 1997. *In*: Proceedings of the Fifth International Symposium on Solid Oxide Fuel Cells (SOFC-V). Aachen, Germany, p.1253.

Paulik, W., Baskaran, S., Armstrong, T.R., 1998. *J. Mater. Sci.*, **33**:2398.

Paulik, S.W., Armstrong, T.R., 2000. *In*: Proceedings of Fourth European Solid Oxide Fuel Cell Forum. Lucerne, Switzerland, p.546.

Pint, B.A., 1996. *Oxid. Met.*, **45**:1.

Pint, B.A., Matin, J.R., Hobbs, L.W., 1993. *Oxid. Met.*, **39**:167.

Quadakkers, W.J., Griner, H., Kock, W., 1994. *In*: Proceedings of the First European Solid Oxide Fuel Cell Forum. Lucerne, Switzerland, **1**:525.

Quadakkers, W.J., Greiner, H., Hansel, M., Pattanaik, A., Khanna, A.S., Mallener, W., 1996. *Sol. Stat. Ion.*, **91**:55.

Quadakkers, W.J., Malkow, T., Albellan, P., 2000. *In*: Proceedings of Fourth European Solid Oxide Fuel Cell Forum. Lucerne, Switzerland, **2**:827.

Redd, D.M., Anderson, H.U., Huebner, W., 1996. *J. Electrochem. Soc.*, **143**:1558.

Sakai, N., Kawada, T., Yokokamo, H., Dokiya, M., Iwata, T., 1990a. *Sol. Stat. Ion.*, **40/41**:394.

Sakai, N., Kawada, T., Yokokawa, H., Dokiya, M., Iwata, T., 1990b. *J. Mater. Sci.*, **25**:4531.

Sakai, N., Kawada, T., Yokokawa, H., Dokiya, M., 1991. *In*: Proceedings of the Second International Symposium on Solid Oxide Fuel Cells. Commission of The European Community, Luxembourg, p.59.

Sakai, N., Horita, T., Yokokawa, H., Dokiya, M., Kawada, T., 2000. *In*: Proceedings of Fourth European Solid Oxide Fuel Cell Forum. Lucerne, Switzerland, **2**:531.

Samsonovin, G.V., 1973. *In*: Turton, C.N., Turton, T.I. (Eds.), The Oxide Handbook. Plenum Press, p.125.

Schmidt, V.H., 1981. Electrical Properties of Lanthanum Chromite Based Ceramics in Hydrogen and Oxidizing Atmospheres of High Temperature. Rept. No. DOE/ET/15415-1, U.S. Department of Energy, Washington D.C.

Simner, S.P., Hardy, J.S., Stevenson, J.W., Armstrong, T.R., 1999. *In*: Proceedings of the Sixth International Symposium on Solid Oxide Fuel Cells (SOFC-VI). Honolulu, Hawaii, p.696.

Simwonis, D., 1997. *J. Mater. Res.*, **12**:1508.

Singhal, S.C., 1999. *In*: Proceedings of the Sixth International Symposium on Solid Oxide Fuel Cells (SOFC-VI). Honolulu, Hawaii, p.39.

Singhal, S.C., 2000. *MRS Bullet*, **25**:16.

Srilomsak, S., Schilling, D.P., Anderson, H.U., 1989. *In*: Proceedings of the First International Symposium on Solid Oxide Fuel Cells. The Electrochemical Society, Pennington, NJ, p.129.

Steele, B.C.H., 1994. *In*: Drake, J.A.G. (Ed.), Electrochemistry and Clean Energy. Royal Society of Chemistry, p.8.

Tai, L.W., Lessing, P.A., 1991. *J. Amer. Ceram. Soc.*, **74**:155.

Takenoiri, S., Kadokawa, N., Koseki, K., 2000. *J. Therm. Spray Technol.*, **9**:360.

Tanner, C.W., Fung, K.Z., Virkar, A.V., 1997. *J. Electrochem. Soc.*, **144**:21.

Tde, H., 1989. Natural Gas Reformed Fuel Cell Power Generation Systems−A Comparison of Three System Efficiencies. Proceedings of the Twenty Fourth Intersociety Energy Convention Engineering Conference. The Institute of Electrical and Electronics Engineers, Washington, D.C.

Tiffee, E.I., Weising, W., Schiessl, M., Greiner, H., 1990. *Ber. Bunsenges. Phys. Chem.*, **94**:978.

Tolochko, S.P., Kononyuk, I.F., 1986. *Neorg. Mater.*, **22**:1696.

Tolochko, S.P., Konyuk, I.F., Ivashkevich, L.S., 1980. *Neorg. Mater.*, **20**:1892.

Tortorelli, P.F., Devan, J.H., 1992. *Mater. Sci. Eng.*, **A153**:573.

Tortorelli, P.F., Natesan, K., 1998. *Mater. Sci. Eng.*, **A258**:115.

Tsukuda, H., Notomi, A., Hisatome, N., 2000. *J. Therm. Spray Technol.*, **9**:364.

Tsuneizumi, H., 1992. Development of Solid Oxide Fuel Cell With Metallic Separator. The International Fuel Cell Conference Proceedings. NEDO/MITI, Tokyo, Japan.

Ueda, M., Taimatsu, H., 2000. *In*: Proceedings of Fourth European Solid Oxide Fuel Cell Forum. Lucerne, Switzerland, **2**:837.

Urbanek, J., Miller, M., Schmidt, H., Llipert, K., 2000. *In*: Proceedings of Fourth European Solid Oxide Fuel Cell Forum. Lucerne, Switzerland,**2**:503.

Vazquez-Navarro, M.D., McAleese, J., Kilner, J.A., 1999. *In*: Proceedings of the Sixth International Symposium on Solid Oxide Fuel Cells (SOFC-VI). Honolulu, Hawaii, p.749.

Virkar, A.V., England, D.M., 2000. Solid Oxide Fuel Cell Interconnector, United States Patent, 6326096.

Virkar, A.V., Kim, J.W., 2001. Planar Solid Oxide Fuel Cell Stack with Metallic Foil Interconnect, United States

Patent, 6106967.

Virkar, A.V., Chen, J., Tanner, C.W., Kim, J.W., 2000. *Sol. Stat. Ion.*, **131**:189.

Warde, C.J., Isenberg, A.O., Brown, J.T., 1976. High-Temperature Solid Electrolyte Fuel Cell Status and Programs at Westinghouse. *In*: Program and Abstracts, ERDA/EPRI Fuel Cell Seminar. Palo Alto, CA.

Webb, J.B., Sayer, M., Mansingh, A., 1977. *Can. J. Phys.*, **55**:1725.

Weber, W.J., Griffin, C.W., Bates, J.B., 1987. *J. Am. Ceram. Soc.*, **70**:265.

Williford, R.E., Armstrong, T.R., 1999. *In*: Proceedings of the Sixth International Symposium on Solid Oxide Fuel Cells (SOFC-VI). Honolulu, Hawaii, p.687.

Wright, I.G., Pint, B.A., Simpson, C.S., Tortorelli, P.F., 1997. *Mater. Sci. Forum.*, **251/254**:195.

Yakabe, H., Yasuda, I., Hishinuma, M., 1999. *In*: Proceedings of the Sixth International Symposium on Solid Oxide Fuel Cells (SOFC-VI). Honolulu, Hawaii, p.677.

Yasuda, I., Hikita, T., 1993. *J. Electrochem. Soc.*, **140**:1699.

Yasuda, I., Baba, Y., Ogiwara, T., Yakabe, H., Matsuzaki, Y., 2001a. *In*: Proceedings of the Seventh International Symposium on Solid Oxide Fuel Cells (SOFC-VII). Tsukuba, Ibaraki, Japan, p.131.

Yasuda, I., Ogiwara, T., Yakabe, H., 2001b. *In*: Proceedings of the Seventh International Symposium on Solid Oxide Fuel Cells (SOFC-VII). Tsukuba, Japan, p.783.

Yokokawa, H., Sakai, N., Dokiya, M., 1991. *J. Electrochem. Soc.*, **138**:1018.

Yoo, Y., Daugo, M., 2002. *In*: Proceedings of the Seventh International Symposium on Solid Oxide Fuel Cells (SOFC-VII). Tsukuba, Ibaraki, Japan, p.837.

Zhu, W.Z., Deevi, S.C., 2003. Oxidation Behavior of Iron Aluminide Alloys In the Operating Temperature Range For Solid Oxide Fuel Cell, Submitted to TMS Spring Conference. San Diego, CA.

Zhuk, P.P., Vecher, A.A., Samokhval, V.V., Naumovich, E.N., Viskup, A.P., 1988. *Neorg. Mater.*, **24**:105.